Article

Advanced State of Charge Estimation Using Deep Neural Network, Gated Recurrent Unit, and Long Short-Term Memory Models for Lithium-Ion Batteries under Aging and Temperature Conditions

Saad El Fallah [1],*, Jaouad Kharbach [1], Jonas Vanagas [2], Živilė Vilkelytė [2], Sonata Tolvaišienė [2], Saulius Gudžius [3], Artūras Kalvaitis [3], Oumayma Lehmam [1], Rachid Masrour [1], Zakia Hammouch [4,5,6], Abdellah Rezzouk [1] and Mohammed Ouazzani Jamil [7]

[1] Laboratoire de Physique de Solide, Faculté des Sciences Dhar El Mahraz, Université Sidi Mohamed Ben Abdellah, B.P. 1796, Fès 30003, Morocco
[2] Faculty of Electronics, Vilnius Gediminas Technical University, 10223 Vilnius, Lithuania
[3] Faculty of Electrical and Electronics Engineering, Kaunas University of Technology, 51347 Kaunas, Lithuania
[4] Division of Applied Mathematics, Thu Dau Mot University, Thu Dau Mot 75100, Vietnam
[5] Department of Medical Research, China Medical University Hospital, Taichung 404327, Taiwan
[6] Département des Sciences, École Normale Supérieure, Moulay Ismail University, Meknes 50000, Morocco
[7] Laboratoire Systèmes et Environnements Durables, Université Privée de Fès, Lot. Quaraouiyine Route Ain Chkef, Fès 30040, Morocco
* Correspondence: saad.elfallah@usmba.ac.ma

Abstract: Accurate estimation of the state of charge (SoC) of lithium-ion batteries is crucial for battery management systems, particularly in electric vehicle (EV) applications where real-time monitoring ensures safe and robust operation. This study introduces three advanced algorithms to estimate the SoC: deep neural network (DNN), gated recurrent unit (GRU), and long short-term memory (LSTM). The DNN, GRU, and LSTM models are trained and validated using laboratory data from a lithium-ion 18650 battery and simulation data from Matlab/Simulink for a $LiCoO_2$ battery cell. These models are designed to account for varying temperatures during charge/discharge cycles and the effects of battery aging due to cycling. This paper is the first to estimate the SoC by a deep neural network using a variable current profile that provides the SoC curve during both the charge and discharge phases. The DNN model is implemented in Matlab/Simulink, featuring customizable activation functions, multiple hidden layers, and a variable number of neurons per layer, thus providing flexibility and robustness in the SoC estimation. This approach uniquely integrates temperature and aging effects into the input features, setting it apart from existing methodologies that typically focus only on voltage, current, and temperature. The performance of the DNN model is benchmarked against the GRU and LSTM models, demonstrating superior accuracy with a maximum error of less than 2.5%. This study highlights the effectiveness of the DNN algorithm in providing a reliable SoC estimation under diverse operating conditions, showcasing its potential for enhancing battery management in EV applications.

Keywords: lithium-ion battery; GRU neural network; LSTM neural network; state of charge; deep learning; electrical vehicle

1. Introduction

Lithium-ion batteries represent a highly effective solution for energy storage devices, despite some significant challenges. Because of the global commitment to reduce greenhouse gas emissions, electric vehicles have become one of the best candidates to gradually replace internal combustion engine vehicles [1]. Nowadays, Li-ion batteries are widely used in most electronic devices and electric vehicles (EVs), as well as in smart grid technology,

this development has led to the V2G (vehicle-to-grid) technology [2,3]. This new technology allows the battery of an electric car to be charged or discharged according to the needs and capacity of an electrical network. Lithium-ion technology offers a number of benefits compared to other energy storage technologies. The importance of lithium-ion batteries in electric vehicles (EVs) continues to grow, thanks to their high energy density, long life, and ability to withstand rapid charge and discharge cycles. An accurate state-of-charge (SoC) estimation is essential for efficient battery management, ensuring the safety, energy efficiency, and durability of the EV [4,5]. A battery management system (BMS) is essential in any application [6], especially in electric vehicles, where it can monitor and protect the battery condition to ensure the reliable, safe, and efficient operation of electric vehicles [7,8]. The BMS is vital for knowing the available energy in the battery and therefore predicting the remaining range of the electric vehicle [9]. However, a direct measurement of the SoC is not possible due to the nonlinearity of the SoC and the complex dynamics of batteries [10,11].

The SoC is determined by the percentage of the current capacity $Q(t)$ compared to the nominal capacity Q_n. The latter is the energy that can be extracted from the battery when it is fully charged [12]; this value is specified by the producer. For battery packs, accurate SoC values for each cell are essential for cell balancing and efficient battery management [13]. One of the classic formulas for calculating SoC is the Coulomb Counting equation, in which the SoC is calculated by integrating the charge/discharge current versus time, which is given as follows:

$$SoC(t) = \left(1 - \frac{\int_0^t i(t)d(t)}{C_n}\right) \times 100\% \tag{1}$$

An accurate SoC estimation is necessary to prevent damage to the battery and unexpected failure by protecting the battery from overcharging and deep discharge [14]. However, the estimation of the SoC remains a major challenge due to temperature variations and aging effects that influence battery performance. The traditional methods of estimating the SoC have significant limitations under these variable conditions. Therefore, several techniques in this regard are used to estimate the SoC for electric vehicle applications [15]. There are many studies on improved SoC estimation approaches that give a robust estimate of the SoC [16], among which the following can be mentioned: electrical measurement only-methods, like the Open-Circuit Voltage (OCV) technique which gives an approximation of the SoC by the monotonic relationship between the SoC and its OCV [17]. Although the Coulomb Counting method, which estimates the state of charge by integrating the discharge current over time, is easy to implement, it requires regular recalibrations because the error in this estimate accumulates over time due to the low accuracy of the current sensor [18]. Various approaches have been developed to estimate the SoC of Li-ion batteries, incorporating different modeling techniques. These include electrical models, which concentrate on representing the battery behavior through circuit-based simulations, and mathematical equation models, which capture battery dynamics using mathematical formulations. In addition, electrochemical models are employed to capture the complex interaction of chemical reactions within the battery [19,20]. Besides these models, filters can be added to correct model uncertainties to achieve acceptable estimation performance [21], like the adaptive unscented Kalman filter (AUKF) [22–24], adaptive extended Kalman filter (AEKF) [25,26], which employs the covariance adaptation-based method, and the ARX based Kalman filter, which have been discussed in the literature to estimate the SoC. In reference [27], an IAUKF method is proposed as a way to improve the accuracy of the SoC estimation of lithium-ion batteries. The results show that the IAUKF approach is highly robust to the noise covariance of the initial measurement. To improve the performance of the conventional SMO for estimation accuracy and ability to track with less ripples, an Adaptive-Gain SMO (AGSMO) is suggested in reference [28]. The authors of reference [29] studied various scenarios in which systematic errors such as voltage sensor bias, current sensor bias, and initial parameter identification errors [30] existed and tested them using an amp-hour (Ah) integration, a dual extended Kalman filter (DEKF) algorithm,

and the extended Kalman filter (EKF). The test showed the robustness of the three algorithms in the scenarios giving different deviations. The SoC can be estimated efficiently using the DEKF algorithm [29], in the case of systematic errors perturbation, since the maximum error of the SoC estimation by the algorithm is less than 3%, which is better than the results obtained using an EKF and Ah integration. In reference [31], the authors proposed a novel adaptive dual extended Kalman filter [32] (ADEKF) to estimate the SoC. The results demonstrated that the algorithm was capable of estimating the SoC. The algorithm could provide a good reference to the battery management system and had good convergence. The estimation error of the SoC was 2.03%. Furthermore, a detailed comparison between two different structures using a neural network (NN) was investigated in reference [33], that is, the direct structure based on NARX-NN with SoC as the network output and the indirect structure using an (RBF)-based NN embedded with UKF (RBFNN-UKF) with the voltage as the output. The RBFNN-UKF indirect estimation demonstrated an interesting superiority over the direct estimation.

The currently available and commonly used algorithms for estimating SoC are KF [34,35], H-infinity filter [36], PF [37], RLS, PI, and SMO. In reference [38], the PF, KF, and H-infinity approaches were compared. The results indicated that the performance of the UKF, CDKF, PF, and H-infinity filters was superior to the other nonlinear filters. In terms of accuracy, PF performed better compared to EKF and was more precise than H_∞. However, the running time was slower for the PF. The results of the experiments indicated good performance in accuracy and runtime for the H-infinite filter. As a result, this method offered a suitable approach towards SoC online estimation. The recursive least squares method enabled a precise calibration of dynamic model parameters and real-time variations while preserving the simplicity of computation. However, in reference [39], Multiple Adaptive Forgetting Factor Recursive Least Squares (MAFF-RLS) estimates were employed for the estimation of the SoC and the cellular model's internal parameters. The KF is currently the most widely used approach for SoC estimation. The EKF is the most commonly used in the literature [40,41] because of its capability to operate on a nonlinear system and due to its simplicity compared to more sophisticated KFs. There exist several different variants of the KF; in reference [42], eighteen different KF types were listed. Regarding performance, the EKF demonstrated high precision. Various approaches, including an adaptive EKF, unscented KF, central difference KF, and Dual EKF were proposed to develop a better EKF and improve its performance. An Artificial Neural Network (ANN) was employed in references [43,44] to estimate the SoC. The neural network (NN) in reference [44] was coupled with a fuzzy model to generate an Adaptive Neuro-Fuzzy Inference System (ANFIS). The method SMO provides good reliability and robustness to modeling errors and uncertainties. However, in reference [15], the SMO method was coupled with a NN algorithm to decrease the error in the estimation of the SoC. Also, in reference [45], the SoC was estimated by an SMO using a standard driving profile. In Reference [46], for the purpose of achieving a solution that is simple and reducing the processing time while obtaining similar performance compared to other popular estimators, a new algorithm based on disturbance observation-based (DOB) was developed. The output of the proposed model demonstrated that the DOB algorithm was able to estimate the SoC with more accuracy than conventional approaches.

Machine learning (ML) methods can also be used to generate a data-driven model [47,48] and identify the nonlinear relationship between the SoC and measurable variables such as current, voltage, and temperature [49–51]. In reference [52], to estimate the thermal and electrical characteristics of lithium-ion battery cells, the authors evaluated the performance of four ML methods (Random Forest Regressor (RFR), linear regression, Decision Tree Regressor (DTR), and K-nearest neighbors regressor) [53]. In that case study, the DTR model gave the best performance. In reference [54], the authors apply a long short-term memory neural network (LSTM). The model based on the LSTM algorithm outperforms several algorithms [54] such as RF, SVR, and simple RNN. The mean absolute error (MAE) of the SoC estimation reaches 0.91%. The proposed method demonstrates satisfactory performance in accuracy and robustness in the case of a battery with different temperature conditions. There are

also other algorithms in the literature to estimate the SoC [9,55], including the support vector machine (SVM) and K-nearest neighbors (KNN) [56] models. In reference [57], the authors proposed a state-of-charge estimation model based on a dynamically driven recurrent network (DDRN). A nonlinear autoregressive architecture with exogenous inputs (NARX) of the DDRN was applied for the SoC and state-of-health (SoH) estimation [58]. A recurrent neural network with long short-term memory (LSTM) and an unscented Kalman filter (UKF) were combined to estimate the SoC of a 18650 lithium iron phosphate battery in reference [59]. The UKF was incorporated into the network to filter the output noise and improve the accuracy of the SoC estimation. The SoC estimate was the model's output, and its inputs were (current, voltage, temperature). The experimental results showed that the proposed model learned the battery dynamics well and offered a good SoC estimation with root-mean-square errors (RMSEs) less than 1.1% and mean errors (MAEs) less than 1%. Thanks to recent advancements in artificial intelligence, data-driven science is garnering increasing interest due to its remarkable advantages in terms of flexibility and adaptability. Moreover, the implementation of this technique is not complicated and demands relatively limited computations [60]. Nevertheless, it differs from other available techniques like electrochemical models or Equivalent Circuit Models which take a long time to be constructed and parameterized manually. To overcome these challenges, this study explores the use of advanced deep neural network (DNN), gated recurrent unit (GRU), and long short-term memory (LSTM) models. These models are capable of capturing complex, nonlinear relationships between input variables (current, voltage, temperature, aging effect) and the SoC, offering higher accuracy. Supervised learning demonstrates the capability to accurately estimate the SoC across a range of ambient temperature conditions. This is particularly advantageous as traditional estimation methods [51] often necessitate the use of distinct models tailored to specific temperature environments [61].

Several interesting and original contributions of this work are highlighted as follows:

- The proposed DNN, GRU, and LSTM networks are trained using large simulation and experimental datasets for the first time to estimate the SoC. Then, the three networks are compared in terms of MAE, MSE, RMSE, and R^2.
- By rigorously testing the models on experimental and simulated data, an accurate estimate of the SoC is obtained. This validation not only confirms the effectiveness of these models but also underlines the potential of simulation to accelerate the development of battery management systems, resulting in significant savings in terms of time and cost.
- This study simulates the effects of aging for different battery types and capacities, under different charge/discharge profiles. By comprehensively examining the impact of aging on SoC estimation, the paper provides crucial information on long-term battery performance, essential for optimizing battery management systems and prolonging lifespan.
- Most existing papers consider only input data (voltage, current, temperature) to estimate the SoC. For the first time, the proposed models for SoC estimation are trained using a diversified dataset including (current, voltage, temperature, and aging effect) as inputs and SoC as output, so the battery can be exposed to varying dynamics.
- The comparison between deep neural networks and recurrent neural networks demonstrates the high precision of the DNN in SoC estimation. This discovery underlines the potential and reliability of the DNN architecture.
- This comparative study of DNN, GRU, and LSTM models aims to identify the architecture that provides the greatest accuracy of SoC estimation performance in various operational scenarios. The aim is to facilitate the subsequent selection of a hybrid model, paving the way for even more reliable and efficient battery management systems.
- Extensive scenario testing incorporating various charge/discharge profiles, operating temperatures, and battery aging effects validates the accuracy and reliability of these models. This comprehensive evaluation guarantees the robustness of these models, essential for practical deployment in a variety of applications.

- Leveraging simulation techniques, the present study offers a cost-effective and rapid approach to testing different battery configurations, management systems, and aging scenarios. By avoiding time-consuming and costly physical testing, this approach accelerates the development and optimization of battery management systems, facilitating rapid innovation in this field.

In this research paper, a comparative analysis of simulation and experimental data for the accurate estimation of the SoC is conducted. This paper is organized as follows: Section 2 presents the proposed models for SoC estimation, followed by an overview and structure of the DNN, GRU, and LSTM algorithms. Section 3 describes the methodology of the simulation and the experimental data treated in this paper and also examines the effect of aging and temperature. The results of the estimation of the SoC and the analysis of the complexity are discussed and presented in Section 4. The conclusions of this manuscript are finally presented in Section 5.

2. Overview of the Proposed Neural Networks and Theoretical Background

The recurrent neural network (RNN), gated recurrent unit (GRU), long short-term memory (LSTM) and deep neural network (DNN) are advanced models that play a crucial role in estimating the state of charge (SoC) of lithium-ion batteries. These models are distinguished by their unique ability to capture the complex, nonlinear relationships between input variables, such as current, voltage, temperature, and the effect of aging, and the SoC output. In this section, an overview of the theoretical principles underlying these neural networks is presented, along with details of the specifics of each model, as well as their effectiveness and limitations in the context of SoC estimation.

2.1. Recurrent Neural Network (RNN)

An RNN is ideal when required to process sequential information like the translation of sentences and production of titles for an input video. An RNN utilizes past data in its internal memory to forecast future outcomes based on previously computed parameters. In contrast to a traditional NN, like feedforward neural networks, which are unable to save past data, the RNN uses past data to process sequential inputs with recurrent units [62]. Figure 1 illustrates the structure of a recurrent unit w.
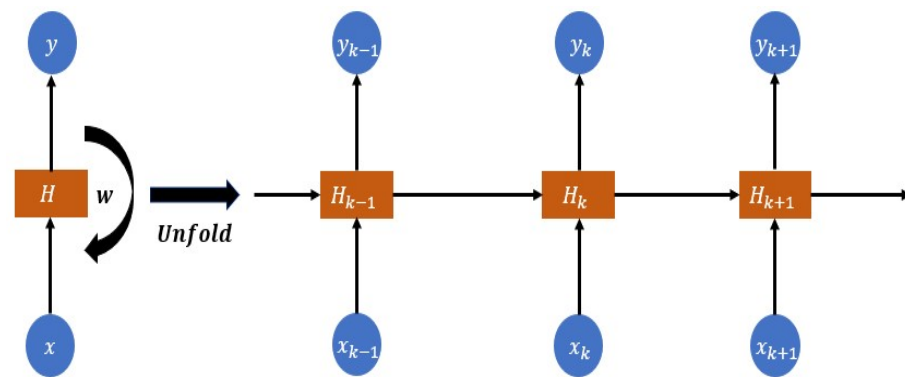

Figure 1. Structure of a recurrent neural network unit (RNN).

The following equation updates the state of each neuron H_k in the hidden layer at each time step:

$$H_k = g\left(w_h \cdot \left[\ H_{k-1} \quad x_k\ \right] + b_h\right) \tag{2}$$

where g denotes the activation function such as a hyperbolic tangent function or a logistic sigmoid function; w_h and b_h are the weight matrix between a hidden layer and an input layer and a bias parameter of the recurrent neuron, respectively. Once the current state H_k is calculated, the output is computed using the following equation:

$$y_k = g\left(w_h \cdot H_k + b_y\right) \tag{3}$$

where b_y and w_h are the bias and the weight matrix between a hidden layer and an input layer, respectively. Since the RNN naturally encodes historical inputs, the network cannot capture all information in the case of a long sequence. In that case, it may lose valuable information from previous time steps. As RNN processes more steps, it suffers more from the fading gradient than other neural network architectures. To solve this problem called gradient vanishing, two popular architectures are used: long short-term memory (LSTM) and gated recurrent unit (GRU). The concept of gradient vanishing refers to the phenomenon where the gradients become increasingly small as they propagate through the layers of the network during training. This can hinder the learning process, particularly in the case of RNNs, or when processing long sequences of data. TensorFlow with the Keras functional API was used in this study to build, test, and train the proposed recurrent neural networks.

2.2. Gated Recurrent Unit (GRU)

The GRU model was developed to give solutions for the long-term dependency problem. A GRU network is created by incorporating a gating mechanism into a basic RNN, enabling it to regulate the flow of information within the neural network. This enhancement allows a GRU network to efficiently capture large step dependencies in time series data and address issues like gradient vanishing or exploding gradients during backpropagation. It employs two gates, the reset gate r, to decide from the previously stored data how successfully the new inputs should be combined, and the update gate z, to set the quantity of information from the past to be let through. In a GRU, the previous hidden state $H_k - 1$ and the current input x_k do not directly affect the current hidden state H_k as in the standard RNN. Figure 2 illustrates the general structure of the GRU [63,64].
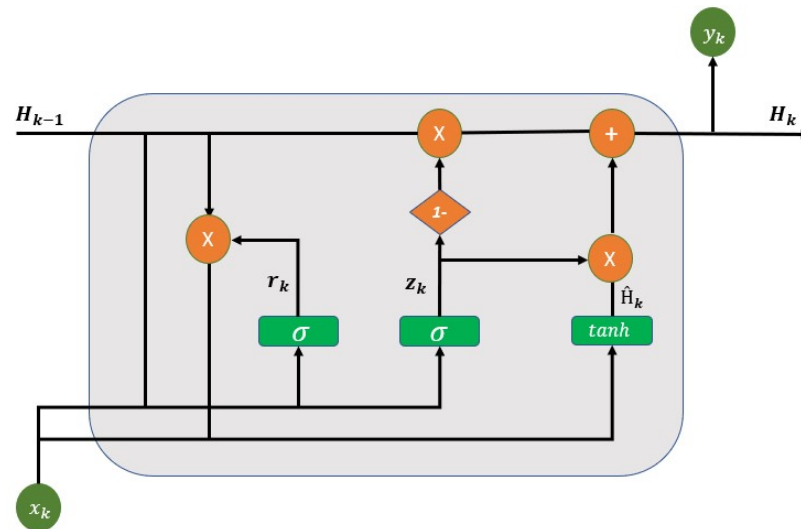

Figure 2. Structure of the gated recurrent unit (GRU).

The GRU activation is a linear combination of the previous state H_{k-1} and a candidate state $\hat{H}_k$:

$$H_k = (1 - z_k) * H_{k-1} + z_k * \hat{H}_k \tag{4}$$

where z_k is called the update gate, which is activated by a sigmoid function:

$$z_k = \sigma(W_z x_k + W_z \cdot H_{k-1} + b_z) \tag{5}$$

The GRU candidate state is calculated as follows:

$$\hat{H}_k = \tanh(W_h x_k + W_h \cdot (r_k * H_{k-1}) + b_h) \tag{6}$$

where r_k is the reset gate activated by a sigmoid function:

$$r_k = \sigma(W_r x_k + W_r \cdot H_{k-1} + b_r) \tag{7}$$

2.3. Long Short-Term Memory Network (LSTM)

The LSTM is a developed type of RNN to solve the gradient vanishing problem. LSTM deals with both short-term and long-term memory and to make the computation efficient and simple, it uses the concept of gates. Unlike an RNN, the LSTM has three types of gates, including the input gate i, the forgetting gate f, and the output gate o. Figure 3 shows a general structure of an LSTM unit [65,66]. The input gate determines what information is stored in the long-term memory. Through this gate, it filters out information from variables that are not useful. The forgetting gate decides which information in long-term memory can be deleted or retained by multiplying the incoming long-term memory by a forgetting vector produced by the current input and the incoming short memory. The output gate uses the current input, the newly computed long-term memory, and the previous short-term memory to generate a new short-term memory to be passed to the cell at the next time step. The output of the current time step can also be taken from this hidden state. The sigmoid function is chosen as the gating mechanism for the three gates due to its ability to produce an output ranging between zero and one. This characteristic influences the flow of information passing through the gates. Additionally, Ref. [67] demonstrates that in large networks, back-propagation learning utilizing antisymmetric activation functions like the hyperbolic tangent function can achieve quicker convergence compared to a similar process employing non-symmetric activation functions such as the sigmoid function [59]. Each part of the cell can be expressed as follows:
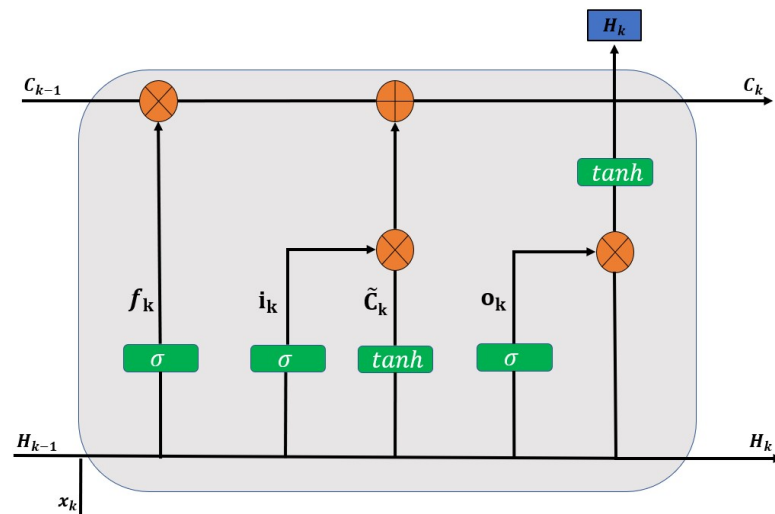

Figure 3. Structure of the long short-term memory (LSTM).

- Calculating the gating units:

$$i_k = \sigma(W_{xi} x_k + W_{Hi} \cdot H_{k-1} + b_i) \tag{8}$$

$$f_k = (W_{xf} x_k + W_{hf} \cdot H_{k-1} + b_f) \tag{9}$$

$$o_k = (W_{xo} x_k + W_{ho} \cdot H_{k-1} + b_o) \tag{10}$$

- Updating memory unit:

$$C_k = f_k C_{k-1} + i_k \tanh(W_{xc} x_k + W_{hc} \cdot H_{k-1} + b_c) \tag{11}$$

- Calculating the output of LSTM unit:

$$H_k = o_k \tanh(C_k) \tag{12}$$

2.4. Deep Neural Networks

Feedforward neural networks are one of the most common networks and offer good predictive performance. A single artificial neuron consists of input nodes and a single output node, which is connected to the input nodes. The output nodes of a hidden layer are connected to the nodes of the following layer with a weight w_{ij} [12]. The total input to a hidden neuron i is computed using the weights and biases of each layer as follows [68]:

$$i_j = \sum_{i=1}^{n} x_i w_{ij} + b_j \tag{13}$$

where i_j represents the total input of the neuron of the hidden layer j, x_i presents the input of the neuron of the hidden layer i and the neuron of the hidden layer j [12], and b_j corresponds to the bias of the neuron of the hidden layer j. Several activation functions can be used on the hidden layer. It is applied to the input and provides the output from the hidden neuron to the following layer as follows:

$$H_j = F(i_j) = \frac{1}{1 + \exp(-i_j)} \tag{14}$$

The MLP model is a feedforward network, which indicates that all layers are connected in a single direction, starting at the input and ending at the output. Figure 4 illustrates a DNN architecture used to estimate the SoC for batteries [51]. The inputs are the temperature, current, and voltage of the battery, while the output is the SoC of the battery. The DNN can accurately and successfully estimate the SoC of a lithium-ion battery [69].
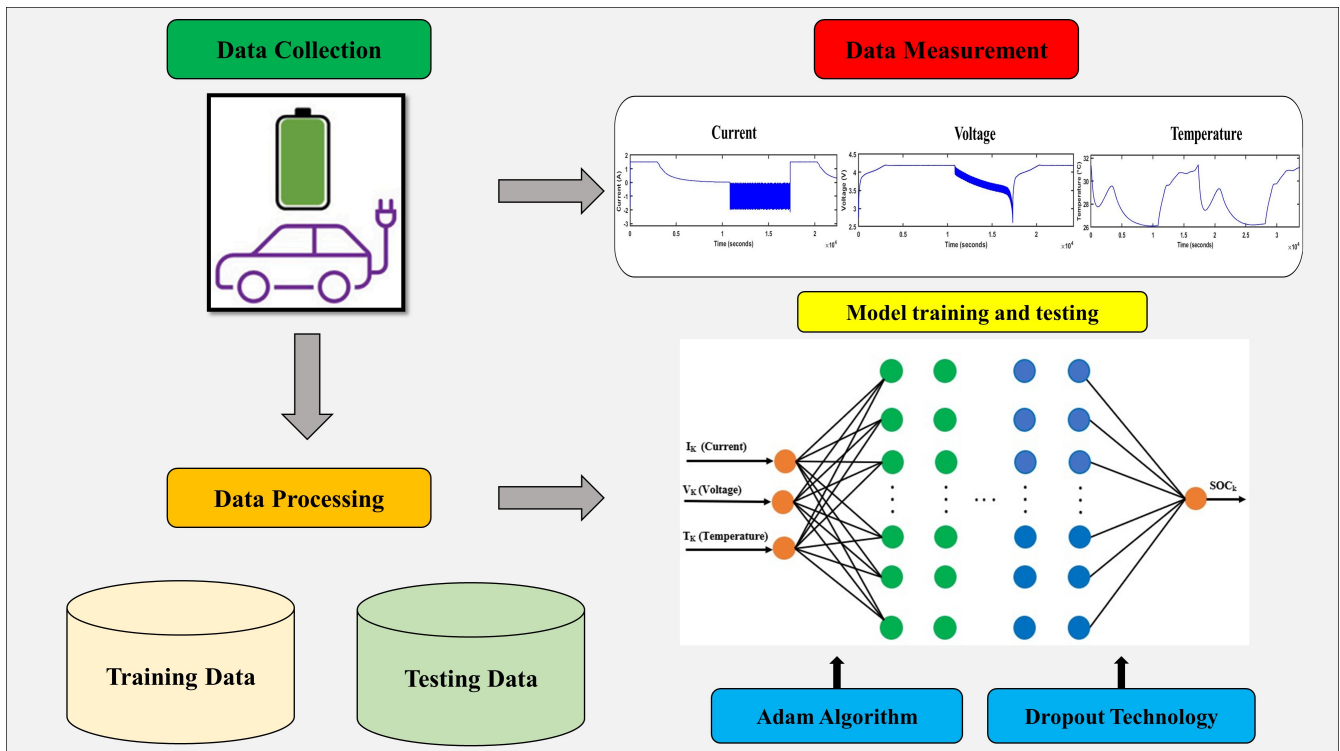

Figure 4. Flowchart of the deep learning process for estimating the state of charge of a Li-ion battery.

Matlab was used to perform this estimation. This software has toolboxes that use neural networks to train the input data and generate an estimation model capable of predicting the SoC of a cell. An application was developed with the main purpose of creating a graphic interface for estimating the SoC with more accuracy. The reason for the development of this application was that the available toolboxes did not incorporate all the

available activation functions. Among these toolboxes, nprtool can be mentioned, which enables to select the number of neurons to be used and to build of a single hidden layer of the feedforward neural network with a sigmoid activation function in the hidden layer and softmax in the output. When this toolbox was tested, it appeared that it did not perform well because it had only one hidden layer and limited activation functions. Therefore, it was necessary to find another one that could be able to simulate multiple hidden layers and various activation functions. For this purpose, the nntool toolbox was useful to simulate what was necessary; however, it was only capable of simulating three activation functions: purelin, tansig, and logsig. The function softmax was not included. Also, it is important to notice that the available toolboxes did not provide a visualization of the training, testing, and validation data plots. Therefore, it was necessary to obtain the indices of data and plot them manually with a script. To be efficient, the proposed application has integrated buttons to perform this operation with a single click. The activation functions tested and added in the application were: poslin, purelin, radbas, logsig, netinv, satlins, softmax, radbasn, satlin, compet, elliotsig, hardlim, hardlims, tribas, and tansig. The proposed multilayer network used the transfer function tansig:

$$\text{tansig}(x) = \frac{2}{1 + \exp(-2x)} - 1 \tag{15}$$

3. Dataset and Experimental Methods

In this article, the lithium-ion cell degeneration datasets utilized, including current, voltage, temperature, and SoC values, were obtained from the NASA PCOE Research Center, including test data for a commercial Li-ion 18650 2 Ah battery [70] for repeated charge and discharge cycles. The battery was charged and discharged using a Constant-Current–Constant-Voltage (CC-CV) profile. NASA has posted two high-throughput datasets containing 62 cells in total on their website. A brief description of the datasets is provided here. The first one (Randomised Battery Usage Data Set) [71] hosted by NASA includes data from 28 Li cobalt oxide 18650 batteries having a nominal capacity of 2.2 Ah. These cells were continuously operated. There are 7 groups of 4 batteries in each group, all cycled at a given ambient temperature (room temperature, 40 °C). The second (Battery Data Set) [70] comprises 34 Li-ion 18650 batteries with 2 Ah of nominal capacity. It was the first publicly accessible dataset on batteries and made a significant impact on the field, providing insight into its influence. The cells were cycled over a range of ambient temperatures 4 °C, 24 °C, and 43 °C, charged using a common CC-CV protocol and with various discharge regimes [72]. To study the effect of operating temperature on the charge/discharge process of a battery, Figure 5 depicts the SoC for different running temperatures at (CC). Initially, the battery was charged with a constant-current profile until the voltage of the cell achieved its nominal voltage, then the battery was charged with a constant-voltage profile until the battery was completely charged. In the discharge phase, a variable-magnitude current profile was applied to completely discharge the battery, as shown in Figure 6a,c. The effect of temperature on the SoC during battery charge and discharge cycles was also taken into account in the simulation [73–75]. Figure 6d illustrates the surface temperature of the battery at room temperature. It is observed that the temperature increases throughout the first segment of the charge and ends with a temperature of about 26 °C. In this study, the experimentally measured SoC was compared with the SoC generated by the simulation. To estimate the simulated and measured SoC, a neural network was tested using both types of data. The training data consisted of 300,000 input voltage, current, and temperature values, and corresponding output SoC values, collected over several charge and discharge cycles. Figure 6a represents a variable current profile during the charging and discharging process, and Figure 6e displays the SoC of the battery as a function of time. It is essential to understand that the SoC is directly influenced by the current profile. When the current is positive (charging), the SoC increases, indicating that the battery is charging. Conversely, when the current is negative (discharging), the SoC decreases, indicating that the battery is discharging. Figure 6e thus reflects the variations in SoC in response to the variations

in current observed in Figure 6a. The models used to estimate the SoC take these current variations into account to provide an accurate estimate of the SoC, which is crucial for efficient energy management and extended lifespan of the battery under real-life conditions. The simulation aimed to train the proposed model at different current profiles to evaluate the robustness of the neural network. Since the experimental data incorporated the effect of temperature on the SoC, the latter was also added to the simulation. To evaluate the effects of various structural aspects of neural networks on the precision of SoC estimation, several tests were carried out. The acquired data were divided into three parts, the first representing 70% for training and the second, with 15%, for testing. Lastly, the final part was used for validation. Furthermore, for the purpose of comparing the SoC obtained by simulation and the experimentally measured SoC, this article used the software Matlab/Simulink R2019a to simulate the discharge and charge pattern for a *LiCoO$_2$* lithium-ion cell. In addition, both types of battery, namely, the Li-ion battery *LiCoO$_2$* and the Panasonic Sanyo UR18650ZY battery, were tested to verify that the proposed algorithms provided highly accurate and reliable estimates, applicable not only to the different conditions described above but also to different batteries. The main chemical specifications used are shown in Table 1. The discharge voltage is affected by the running temperature. At higher temperatures, the discharge voltage increases. On the other hand, as the temperature drops, the discharge time also diminishes.
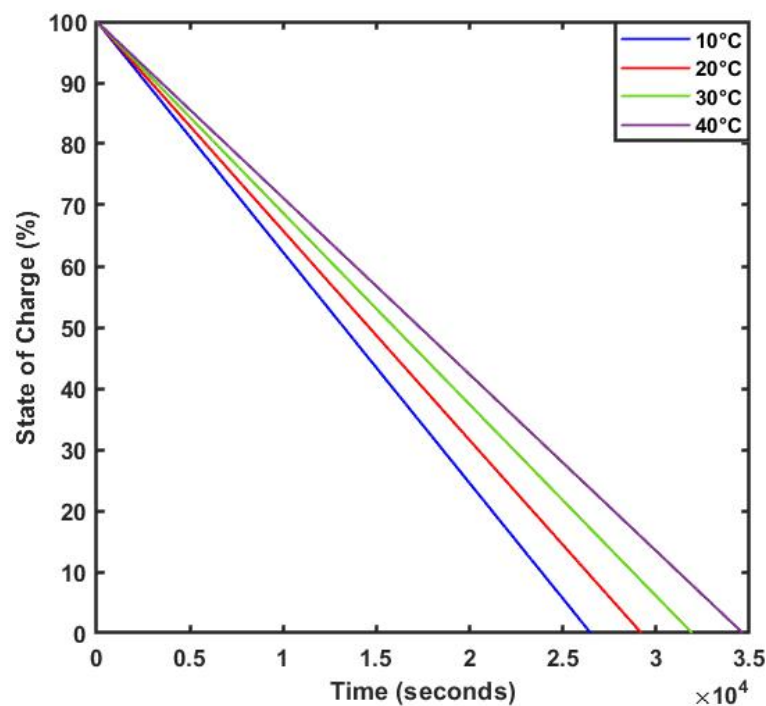

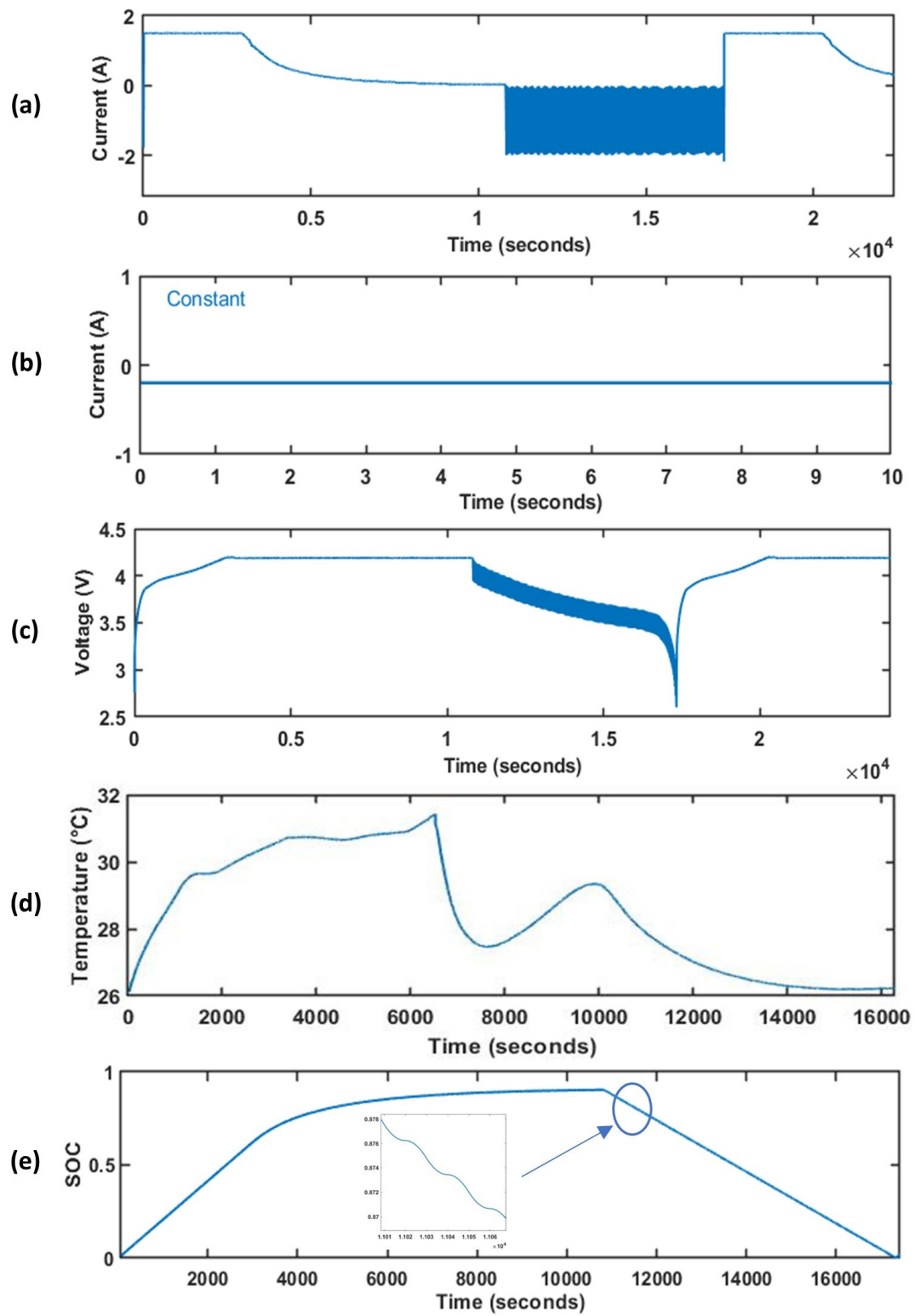**Figure 5.** State of charge for different operating temperatures.

Figure 6. Charging/discharging profiles.

Table 1. Chemical specifications of *LiFePO₄*, *LiCoO₂* and *LiNiO₂* batteries.

Battery	*LiFePO$_4$*	*LiCoO$_2$*	*LiNiO$_2$*
Rated capacity	2.3 Ah	2.05 Ah	3.6 Ah
Nominal voltage	3.4 V	3.3 V	3.1 V
Fully charged voltage	3.7 V	4.2 V	3.7 V
Cut-off voltage	2.4 V	2.5 V	2.3 V
Nominal discharge current	2.3 A	1.9 A	0.7 A
Capacity at nominal voltage	2.2 Ah	1.8 Ah	2.8 Ah
Initial cell temperature	20 °C	20 °C	20 °C
Operating temperature	20–65 °C	20–65 °C	20–65 °C

3.1. Effect of Aging on Various Types of Batteries

The aging manifests itself as a decrease in the nominal capacity of the battery, which means that it cannot store as much energy as before. It is important to note that the aging of li-ion batteries cannot be reversed, but it can be slowed by taking care of the battery and avoiding usage patterns that can damage it [76]. This loss of capacity is due to several factors, including the formation of deposits on the electrodes that can reduce the efficiency of the electrochemical reaction needed to store and release energy [77,78], and the degradation of the electrolyte, which allows lithium ions to move between the battery's electrodes. Over time, the electrolyte can degrade, which can reduce the efficiency of the battery. In addition, the degradation of battery components over time can cause the battery voltage to change, which can affect the accuracy of the battery's SoC estimate [79]. If the state-of-charge estimate is incorrect, it can negatively impact the performance and life of the battery. Matlab/Simulink is a useful tool to simulate the effect of aging of a battery to increase the number of cycles, simulate various situations, save a lot of time, and have a good understanding of the behavior of a battery during aging and under different temperature values [80]. Figure 7 represents the aging effect of various battery types with different chemical specifications (see Table 1) at a constant charge/discharge current profile.

If the effect of aging is not taken into account when estimating the battery's state of charge, it can lead to significant errors in the measurement of the battery's actual capacity. It is therefore essential to take into account the effect of aging to maximize the life of the battery and avoid overcharging or deep discharges that can damage it. This is especially important for critical applications, such as electric vehicles, medical devices, and energy storage systems [81]. Figure 8 illustrates the aging effect of the battery at a variable charge/discharge current profile.

The temperature can significantly impact the performance and life of lithium-ion batteries. In general, Li-ion cells perform best at temperatures between 20 and 25 °C. When the temperature rises above 30 °C, the battery's capacity can decrease, reducing its life span. On the other hand, when the temperature is too low, below 0 °C, the capacity of the battery can also decrease, reducing its life [82]. In addition, at low temperatures, the electrochemical reaction process becomes slower, which can lead to uneven distribution of lithium on the anode, resulting in the formation of lithium dendrites. These structures can puncture the separator and cause internal short-circuits, leading to irreversible battery degradation. Reducing the temperature increases the internal resistance of the battery, reducing the efficiency of the electrochemical reaction and resulting in a loss of usable capacity. This increase in internal resistance subjects the battery to additional stress during charge and discharge cycles, accelerating the aging of the active materials and separator. Low temperatures can cause electrolyte components to precipitate, reducing its ability to conduct lithium ions between electrodes. Electrolyte degradation leads to a reduction in battery capacity and an increase in internal resistance, accelerating the aging process [83]. Low-temperature thermal cycling can cause electrode materials to expand and contract, leading to cracking and delamination. This structural damage reduces the battery's ability to maintain an efficient electrochemical reaction, contributing to lower capacity and shorter

service life. When charging, a higher temperature can allow for faster charging and greater storage capacity. However, too high a temperature can shorten the life of the battery and increase the risk of overheating or explosion. When discharging, a higher temperature can also improve the performance of the battery but may shorten its life. In general, it is recommended that a stable and moderate operating temperature be maintained for optimum performance and maximum life of the lithium-ion battery [84].
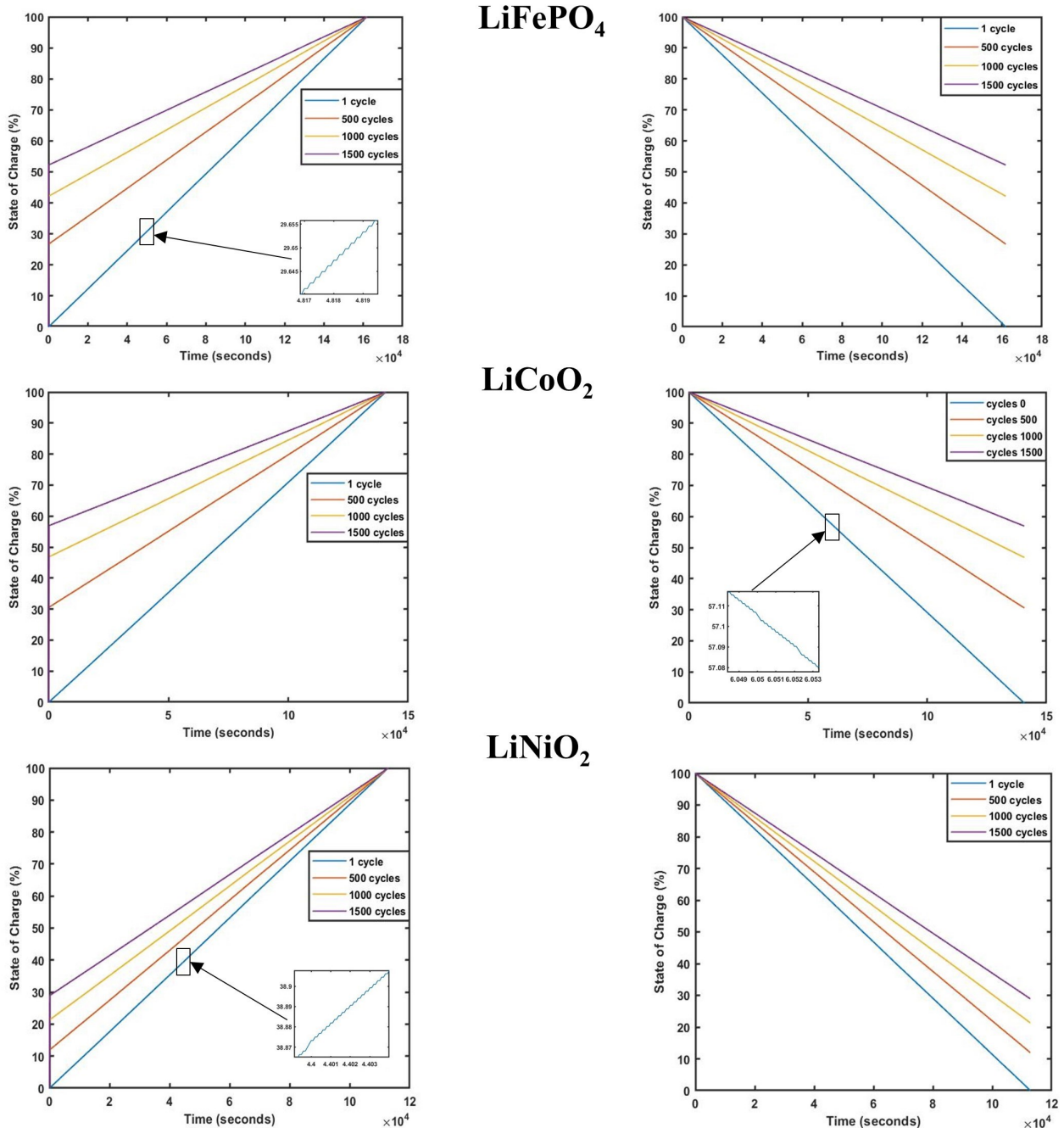

Figure 7. Effect of aging on different types of batteries of different capacities for a constant charge/discharge current profile.
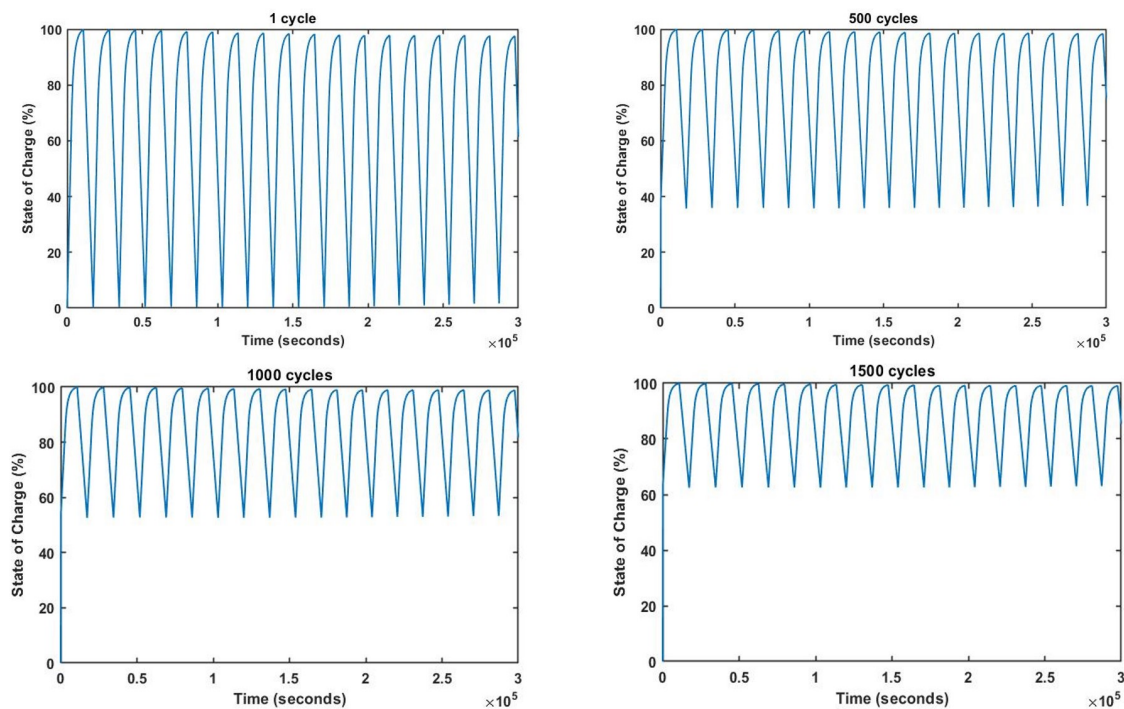
Figure 8. Effect of aging of a *LiCoO₂* battery for a variable charge/discharge current profile.

3.2. Effect of Operating Temperature

The operation of an electrochemical system at elevated temperatures can have several effects on the electrochemical reactions that take place during charging and discharging. One of the most important consequences is that the discharge reaction can be faster at higher temperatures. On the other hand, the speed of the charging reaction can also be increased, which means that the battery can be charged more rapidly [85].

4. Experimental Results and Discussion

4.1. Results of the Estimation Obtained at Constant Current without Aging Effect

The training data included 110,985 samples of current, voltage, temperature, and corresponding SoC values obtained from several charging and discharging processes of a Panasonic Sanyo UR18650ZY commercial battery cell (PANASONIC & SANYO, Osaka, Japan) with a nominal voltage of 3.7 V and a nominal capacity of 2.6 Ah. The battery was charged using a constant current and voltage (CC-CV) profile and then fully discharged until the voltage reached 2.5 V. The manufacturer claimed a lifespan of 300 charge and discharge cycles under specified conditions. The main chemical specifications are indicated in Table 2.

Table 2. Chemical characteristics of the battery.

Battery	Panasonic Sanyo UR18650ZY
Cathode	*LiNiCoAlO₂*
Anode	Graphite
Rated capacity	2.6 Ah
Nominal voltage	3.7 V
Fully charged voltage	4.2 V
Cut-off Voltage	2.5 V
Initial cell temperature	20 °C
Operating temperature	20 °C to 65 °C

The collected data were then divided into three sets: 15% was used for testing, 15% for validation, and the remaining 70% for training the proposed neural networks. To extract

these data during the charging and discharging process, an experimental device was established to collect all data. This setup consisted of a battery, a battery charger, a DC load (discharge), a current sensor (ACS712), a voltage sensor (from DCT electronic), a temperature sensor (LM35DZ), a breadboard, and an Arduino Uno card, as represented in Figure 9.
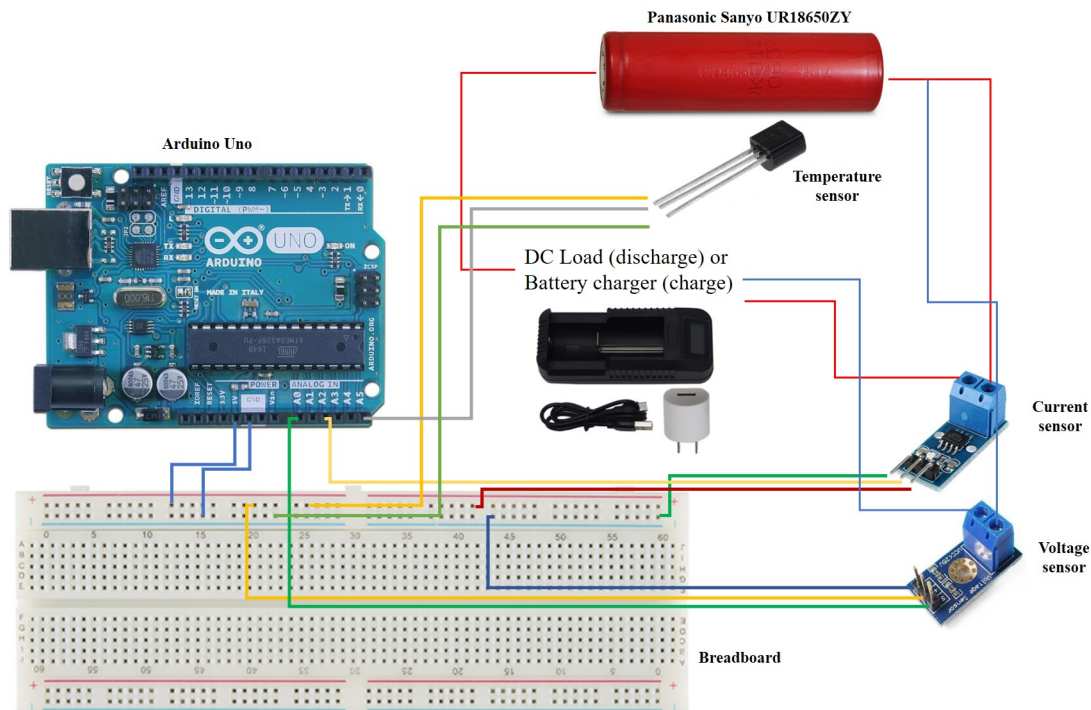

Figure 9. Instrumentation platform to collect electrical and thermal data for a battery experiment.

Figure 10 illustrates the precision of the proposed models in predicting the SoC. The results indicate that the neural networks accurately estimated the battery's SoC, with a maximum error of under 4% and an average error of less than 2%. Table 3 presents the SoC prediction errors for the various proposed models.

Table 3. State of charge prediction errors for the different proposed models

Model	RMSE (%)	MAE (%)	MSE (10^{-3})	R^2
DNN	0.290	0.190	0.008	0.9999
GRU	3.379	1.047	1.140	0.9828
LSTM	3.797	1.198	1.440	0.9773

4.2. Results of the Estimation Obtained at Variable Current without Aging Effect

An accurate and efficient comparison of the experimentally measured SoC of a lithium-ion 18650 cell from the NASA PCOE research center and the simulated SoC of a $LiCoO_2$ battery (see reference [43]) was performed. The results indicated a perfect correspondence between both strategies. These two strategies should be subjected to the same current profile and tested under the same conditions. In addition, the performance of the proposed neural network was tested with both types of data mentioned above and with the same current profile, as shown in Figure 6a. The experimental charge and discharge cycles were simulated using the software mentioned above, taking into account the effect of the operating temperature applied to the SoC of a $LiCoO_2$ cell. The collected data were subsequently used for testing and validating the performance of the proposed DNN, GRU, and LSTM networks. The results of the SoC prediction in two distinct scenarios are discussed. There are several reasons why a comparative study of simulation and experimental data is interesting for the SoC estimation using DNN, GRU, and LSTM. First,

experimental data can provide accurate information about the actual battery behavior, while simulation data can be used to generate larger and more diverse datasets, which can improve the performance of machine learning models. Moreover, simulation data serve the purpose of replicating scenarios challenging or even impossible to emulate through experimentation, such as extreme charge and discharge conditions. Through the comparison of results from experimental and simulated data, it is possible to validate the efficacy of deep learning models and identify the most reliable for estimating the SoC. This combination offers a comprehensive understanding of a battery's potential and constraints, facilitating the refinement of SoC estimation algorithms for enhanced accuracy and reliability.
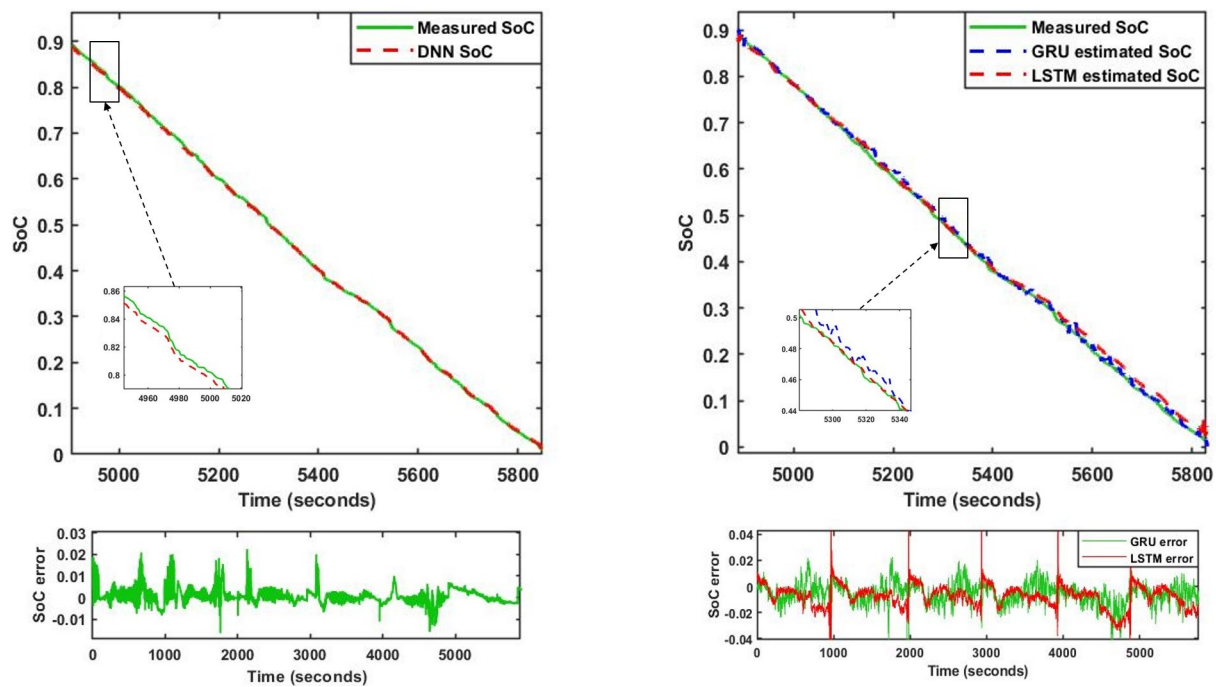

Figure 10. SoC estimated vs. measured SoC and estimation error on the Panasonic Sanyo UR18650ZY battery validation dataset. The DNN network consisted of three layers and nine neurons in each layer.

In the first scenario, experimentally measured data were used to train and validate the proposed models. Then, in the second scenario, the data obtained from the simulation were used to validate the effectiveness of the proposed model in estimating the SoC on the one hand, and on the other hand, to confirm the reliability of the simulation data to train and validate the discussed models. Figures 11 and 12 demonstrate the utilization of a four-layer DNN architecture. In that configuration, the initial three layers consisted of nine neurons each, with the final layer containing a single neuron. The performance evaluation of the network revealed that the predicted SoC, denoted in red, closely followed the reference SoC depicted in blue. The DNN results indicated a mean error of under 0.5% for the experimental data and a maximum error of less than 2.4%. Additionally, simulation data exhibited a mean error below 0.4% and a maximum error under 2.5%. The slight variance in precision observed between the simulation and experimental tests of the DNN could be attributed to the utilization of a new battery in the simulation, as opposed to the battery employed in the experimental setup. The latest results demonstrated that the DNN model provided a reliable estimate of the SoC. To evaluate the performance of that method, the MAE [86], MSE, RMSE [87], and coefficient of determination R^2 were used, which were obtained by calculating predicted and real values. They were used to assess network performance. In the following, n represents the overall sample size, the ith real and predicted values of the target variable are denoted by Y_i and $\widehat{Y}_i$, respectively, and $\overline{Y}_i$ corresponds to the mean value of the observations. The MSE is expressed by the following formula:

$$\text{RMSE} = \sqrt{\frac{1}{n}\sum_{i=1}^{n}\left(Y_i - \widehat{Y}_i\right)^2} \tag{16}$$

The variation in MSE at different epochs for the training, test, and validation datasets is illustrated in Figures 13a and 14a. The best performance of the model is represented by the green circle. Figures 13b and 14b illustrate the error histograms from various datasets. These two figures demonstrate that errors approached zero. These corresponded to the difference between the DNN outputs and targets. The findings presented in Figures 13 and 14 were generated by a four-layer DNN, the first three of which contained nine neurons while the last consisted of one neuron. In that case, the target was the SoC calculated from simulation and experiment, respectively.
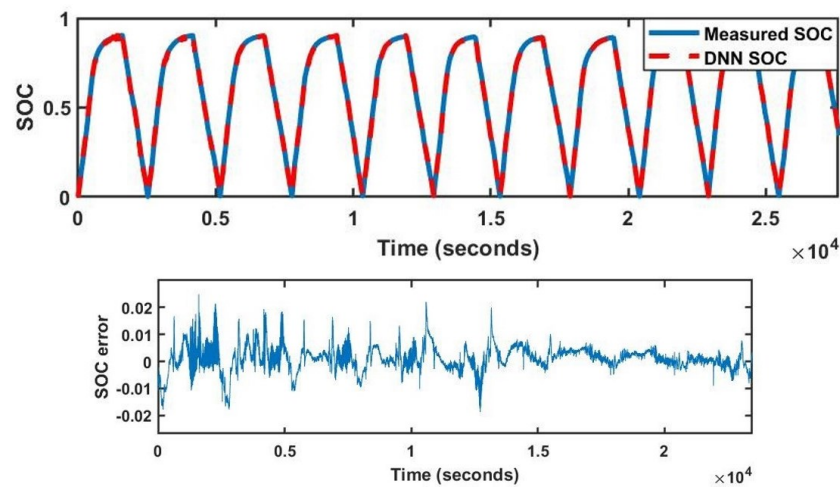

Figure 11. The SoC predicted by the DNN compared to the real SoC and the error of estimation on the Li-ion 18650 battery validation dataset. The DNN was composed of three layers with nine neurons in each layer.
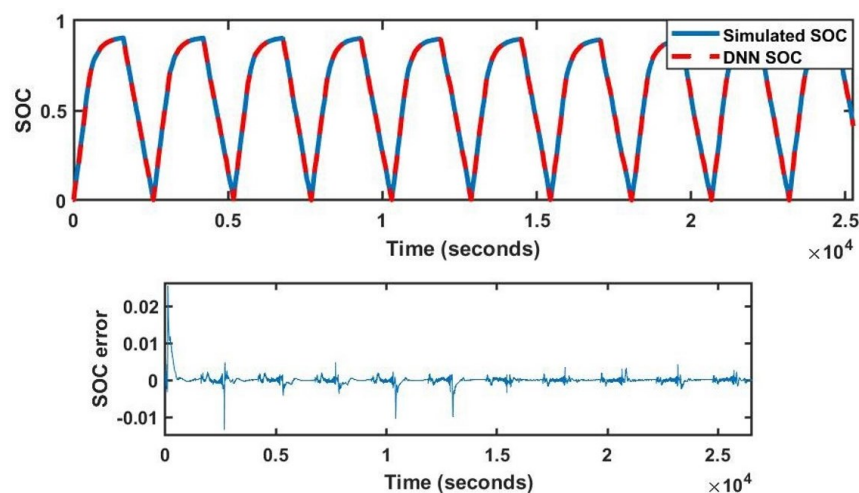

Figure 12. SoC estimated by the DNN compared to the simulated and error of estimation on the Li-ion battery *LiCoO₂* validation dataset. The DNN was composed of three layers with nine neurons in each layer.
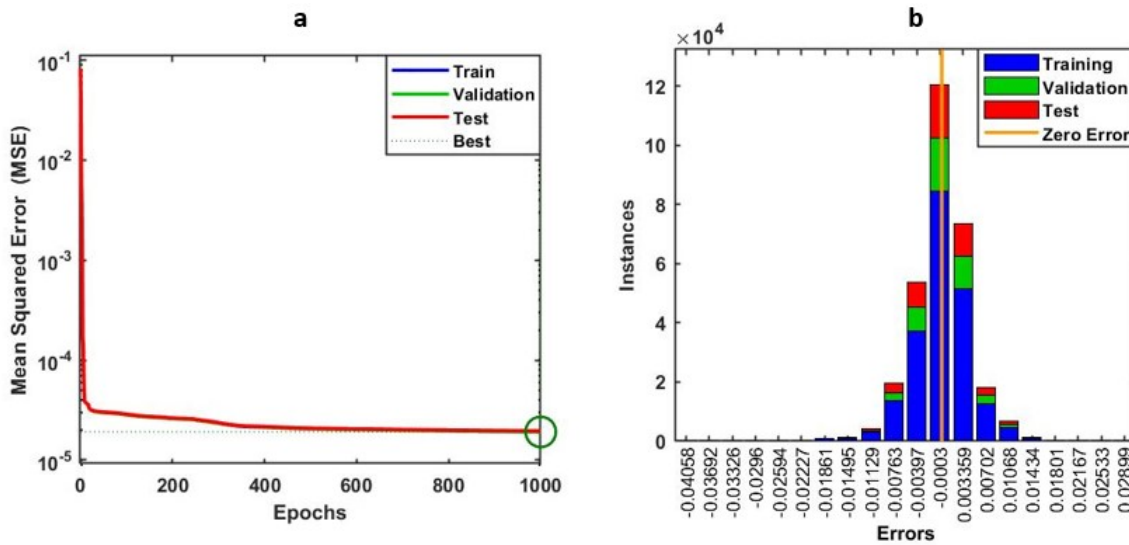
Figure 13. (**a**) Mean square error for training, testing, and validation datasets for different epochs. (**b**) Error histogram of the difference between the target and the DNN output.
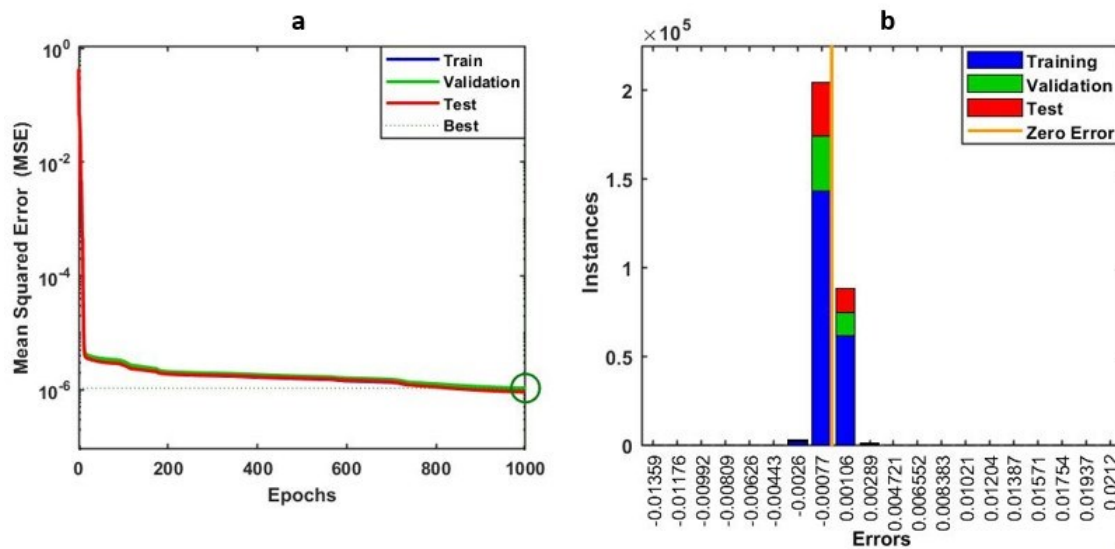

Figure 14. (**a**) Mean square error for the training, testing, and validation datasets for different epochs. (**b**) Error histogram of the difference between the target and the DNN output.

Figures 15 and 16 show the SoC estimation results for the two types of experimental and simulation data, respectively. Both approaches were subject to the same current profile mentioned above. The two models were capable of estimating the SoC successfully, but the LSTM offered a slight improvement compared to the GRU. A nonlinear transformation of the input data was performed by two stacked hidden layers, the first of which contained 64 units and the next 32. An activation function, the hyperbolic tangent (Tanh), which converts values varying from −1 to 1, was integrated into both layers. The purpose of this was to ensure that the output of the neurons did not become too large, since this would have necessitated more calculation time and memory. The 20% dropout regularization was applied between hidden layers to prevent overfitting and enhance network generalization. The Adam optimizer was used to minimize the loss function [88], and the learning rate was set to 10^{-3}. For experimental data, the GRU provided a mean error value under 2.2% and a maximum error value under 4.6%, while for simulation data, it provided a mean error value under 2.4% and a maximum error value under 5.4%. In contrast, the LSTM provided a mean error value under 2.2% and a maximum error value under 5.5% for experimentally acquired data, and a mean error value under 2.4% and a maximum error

value under 4.4% for simulation-generated data. Table 4 displays the statistical metrics obtained for both models using the two data sources. The DNN model performed better than the LSTM and GRU ones in terms of RMSE, MAE, and MSE values of 0.341%, 0.463%, and 0.21×10^{-4}, for data obtained experimentally, respectively, and for data generated by simulation, the RMSE, MAE, and MSE values were 0.107%, 0.040%, and 0.011×10^{-4}, respectively. In addition, the R^2 value of DNN was higher than that of the GRU and LSTM models, demonstrating the precision of that model for estimating the SoC. Figures 17 and 18 represent the training and validation losses of the GRU and LSTM models for simulation and experimental data.
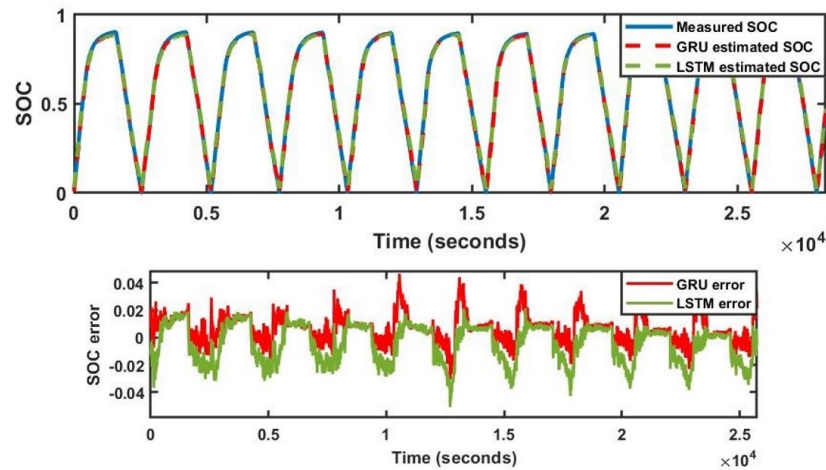

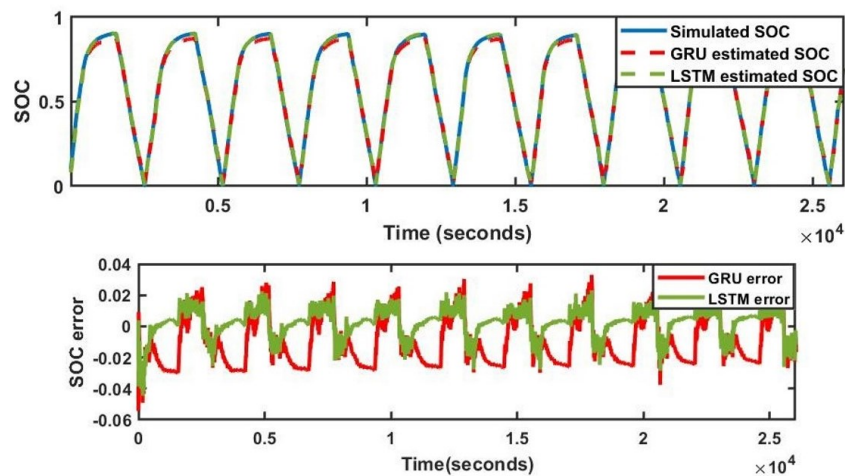**Figure 15.** GRU and LSTM validation results for experimental data.

Figure 16. Validation results of GRU and LSTM models for simulation data.

Table 4. State of charge prediction errors for the different proposed models under two different conditions.

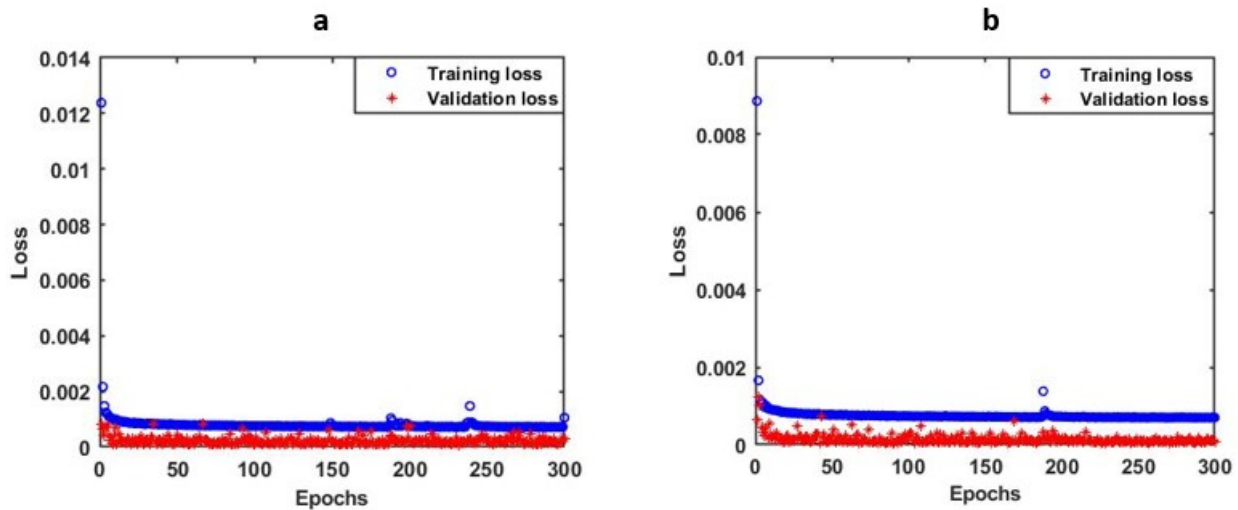| Model	Validation Data	RMSE (%)	MAE (%)	MSE (10^{-4})	R^2
DNN	Experimental	0.463	0.341	0.210	0.9999
	Simulation	0.107	0.040	0.011	0.9999
GRU	Experimental	1.152	0.862	1.320	0.9976
	Simulation	1.700	1.517	2.890	0.9973
LSTM	Experimental	1.411	1.085	1.990	0.9989
	Simulation	0.900	0.774	0.081	0.9993

Figure 17. Training and validation loss of the (**a**) gated recurrent unit (GRU) model and (**b**) long short-term memory (LSTM) model for experimental data.
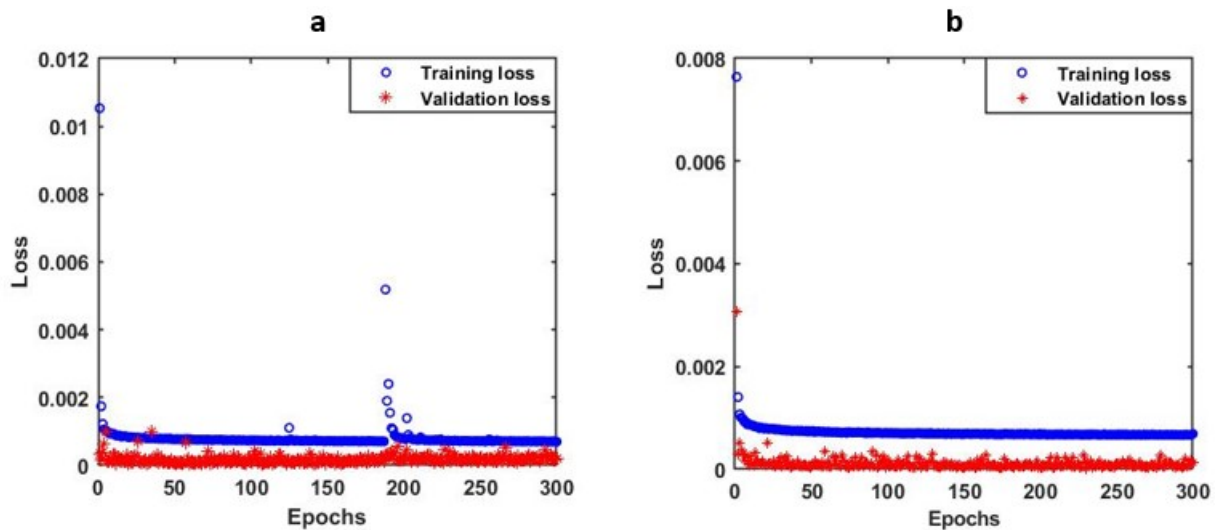

Figure 18. Training and validation loss of the (**a**) gated recurrent unit (GRU) model and (**b**) long short-term memory (LSTM) model for simulation data.

The convergence of the networks demonstrated the performance of the proposed models in learning the SoC estimation problem. Figures 19 and 20 show the offset between the reference SoC of each of the two types of data (experimental and simulation) and the predicted SoC. Although all three models were successful in estimating the SoC in both charge and discharge phases, the DNN model had a significant advantage over the GRU and LSTM models with a maximum error of 2.5% compared to 4.6% for the GRU and 5.5% for the LSTM. The difference in error between GRU and LSTM models came from the difference in the total number of parameters in the two models, which was 22,689 in the GRU versus 29,857 parameters in the LSTM model. The superiority of the DNN over the GRU and LSTM models in state-of-charge (SoC) estimation hinges on various factors, such as the nature of the problem at hand, the volume and quality of the training data, the model's complexity, and the optimization algorithm employed. A DNN exhibits enhanced capability in capturing intricate correlations between inputs and outputs, but it also has a higher risk of overfitting. Table 5 summarizes the advantages and disadvantages of the three prediction models for reliable battery SoC estimation. To examine the model performance under different conditions, a current profile that simulated real-life situations, like instantaneous braking and acceleration of electric vehicles, was used.

This current profile, illustrated in Figure 21, represents rapid and sudden variations in battery operating conditions, which are relevant external factors but were not included in the initial training dataset. The performance of various SoC methods is summarized in Table 6. The results presented in Figure 22 demonstrated the robustness of the model in the face of a variety of scenarios. The maximum estimation error was less than 0.8%, the mean error was less than 0.3%, and the coefficient of determination was 99.99%. These exceptional performance values attest to the ability of the model to adapt effectively to rapid temperature fluctuations and unexpected load conditions, reinforcing its robustness and reliability in realistic situations. The parameters used to obtain the experimental results are shown in Table 7.
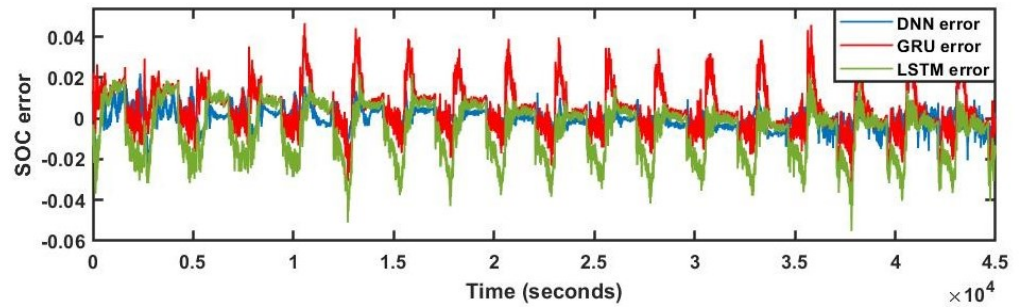
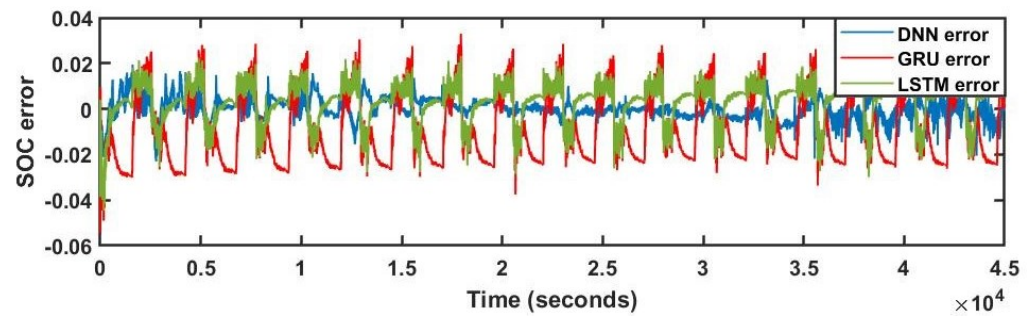**Figure 19.** Estimation error for experimental data.

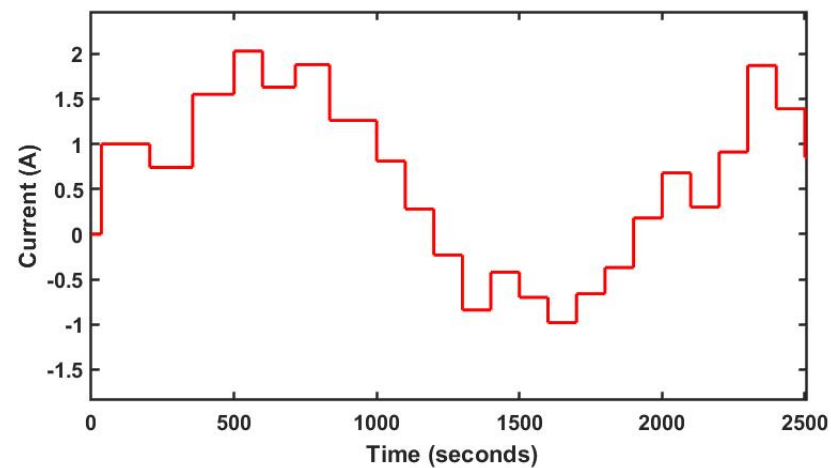**Figure 20.** Estimation error for simulation data.
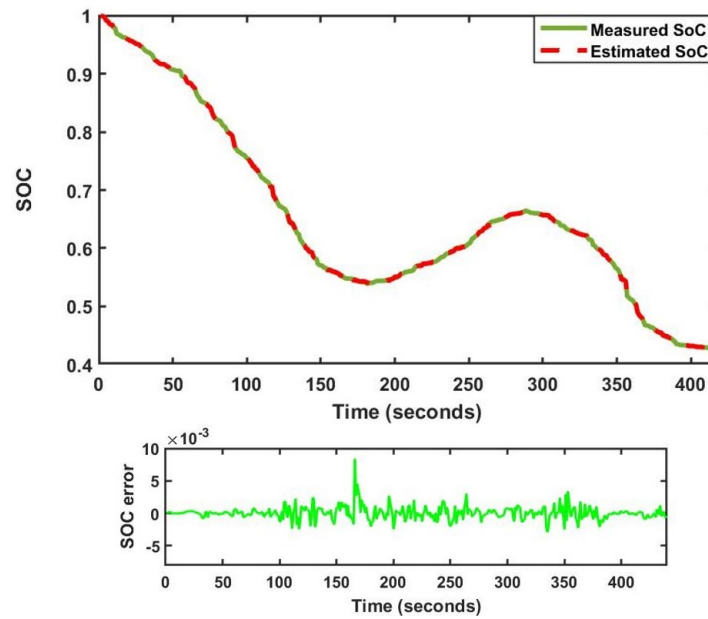
Figure 21. Current profile.

Figure 22. Deep neural network estimated SoC vs. reference SoC and estimation error on the validation dataset.

Table 5. The advantages and disadvantages of the three neural networks for reliable battery SoC estimation.

Model	Advantages	Disadvantages
DNN	- Ability to model complex relationships between inputs (voltage, current, temperature) and outputs. This is useful for capturing nonlinear battery behavior. - Efficient training on big data, an advantage when datasets are large, used to improve the accuracy of SoC estimation. - Data adaptability: the DNN can adapt to different types of data. Lithium-ion batteries vary considerably in terms of manufacturer specifications, operating temperature, charge/discharge cycles, and various conditions of use.	- Massive data requirements: DNN often requires a large quantity of data to generalize correctly, which can be a drawback if the available data are limited. - Data sensitivity: DNN can be sensitive to the data provided, which means that the quality and representativeness of the data used for training are crucial. - Sensitivity to hyperparameters: DNN has many hyperparameters (number of layers, number of neurons for each layer, learning rate, activation function, number of epochs, optimization algorithms like Adam, RMSProp and SGD, regularization to avoid overfitting, etc.).
GRU	- Modeling sequences: the GRU is designed to treat sequential data efficiently, making them suitable for SoC estimation, because they can take into account variations in voltage, current, and temperature over a given period. - Less complex than LSTM: the GRU has a simpler structure than LSTM, which can facilitate learning and reduce the risk of overfitting on small datasets.	- Limitation of short-term memory: although GRU has short-term memory, it may have difficulty capturing long-term dependencies in sequential data.
LSTM	- Capturing long-term dependencies: the LSTM network is designed to capture long-term dependencies in sequences, where the behavior of charging and discharging can be influenced by complex factors over long periods; this capability is crucial. - The LSTM network is better equipped to avoid the problem of gradient disappearance over long sequences, which is common in temporal data.	- Complexity of training: an LSTM network is more complex than a GRU, which can make learning more difficult and require more computing resources. - Risk of overfitting: as a LSTM network has more parameters due to its complexity, the risk of overfitting is higher, especially with limited datasets.

Table 6. Performance of different SoC methods.

Method	Error	Error Calculation Methods	SOC Profile	References
RF	2.63%	MAE	Discharge	[54]
EKF	1.31%	MAE	Discharge	[46]
DOB	0.72%	MAE	Discharge	[46]
SVR	5.19%	MAE	Discharge	[54]
SimpleRNN	1.30%	MAE	Discharge	[54]
GRU-RNN	2.53%	MAE	Discharge	[63]
RNN	2.50%	MAE	Discharge	[63]
DAE-GRU	1.59%	MAE	Discharge	[63]
DNN proposed	0.19%	MAE	Discharge	-
GRU proposed	1.04%	MAE	Discharge	-
LSTM proposed	1.19%	MAE	Discharge	-
AUTOENCOD-LSTM	0.93%	MAE	Discharge	[89]
LSTM-AHIF	1.18%	MAE	Discharge	[90]
LSTM	2.36%	MAE	Discharge	[90]
TBCC-AEKF	2.51%	MAE	Discharge	[91]
TBCC-APF	1.36%	MAE	Discharge	[91]
APF	4.62%	MAE	Discharge	[91]
ACKF-QR-H∞	2.42%	MAE	Discharge	[92]
AEKF	7.26%	MAE	Discharge	[91]
UKF	1.05%	MAE	Discharge	[38]
AEKF	5.80%	MAE	Charge/discharge	[93]
SVM	16.10%	MAE	Charge/discharge	[93]
LSTM-TL	3.80%	MAE	Charge/discharge	[93]
DNN proposed	0.34%	MAE	Charge/discharge	-
GRU proposed	0.86%	MAE	Charge/discharge	-
LSTM proposed	1.08%	MAE	Charge/discharge	-
ANN	3.80%	MAE	Charge/discharge	[94]

Table 7. Description of parameters for gated recurrent unit (GRU) and long short-term memory (LSTM) models.

Parameter	GRU	LSTM
Number of layers	2	2
Layer size	64, 32	64, 32
Dropout	0.2	0.2
Batch size	64	64
Epochs	300	300
Learning rate	0.001	0.001
Optimizer	Adam	Adam
Loss function	MSE	MSE
Number of parameters	22,689	29,857
Reason for difference	GRU has two gates (reset and update).	LSTM has a more complex structure with forget, input, and output gates.

4.3. Results of the Estimation Obtained for Constant Current and Variable Current with Aging Effect

Figures 23–25 demonstrate that the effect of battery aging could affect the quality of the electrical and thermal data provided to the GRU, LSTM, and DNN neural networks, which might result in a decrease in their performance. The effect of battery aging can cause a decrease in the capacity of the battery, therefore reducing its life. This may impact the performance of neural networks, as these models are very sensitive to voltage and current

variations, which may introduce computational errors. A decrease in performance can result, as the models can no longer produce accurate predictions or satisfactory results. In addition, the effect of aging can also affect the stability of electronic components, which can lead to failures and computational errors. Neural networks need a stable and reliable power supply to function properly, and the effect of aging can reduce this stability, resulting in decreased performance.
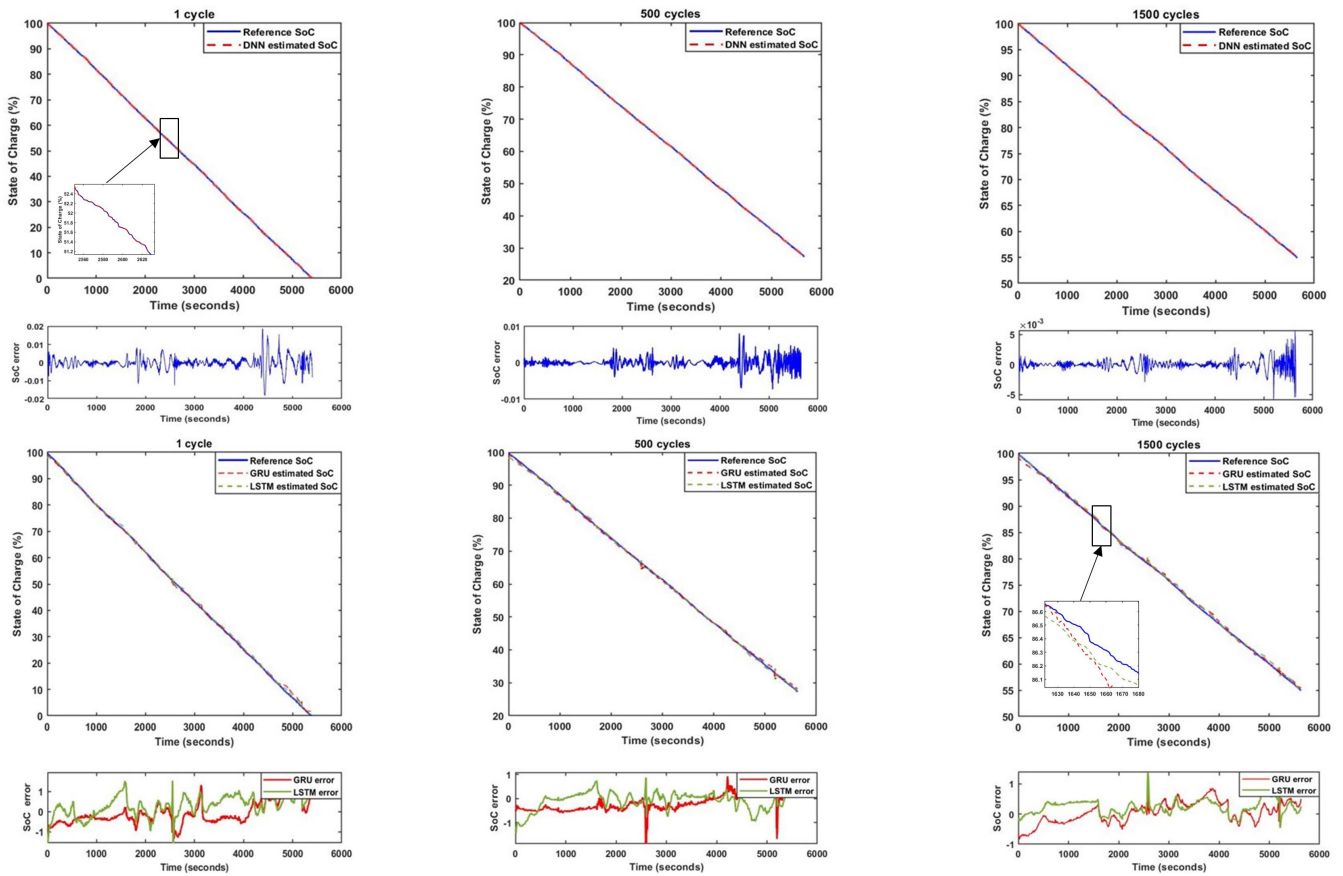

Figure 23. Estimation of the SoC obtained at constant current with the aging effect.
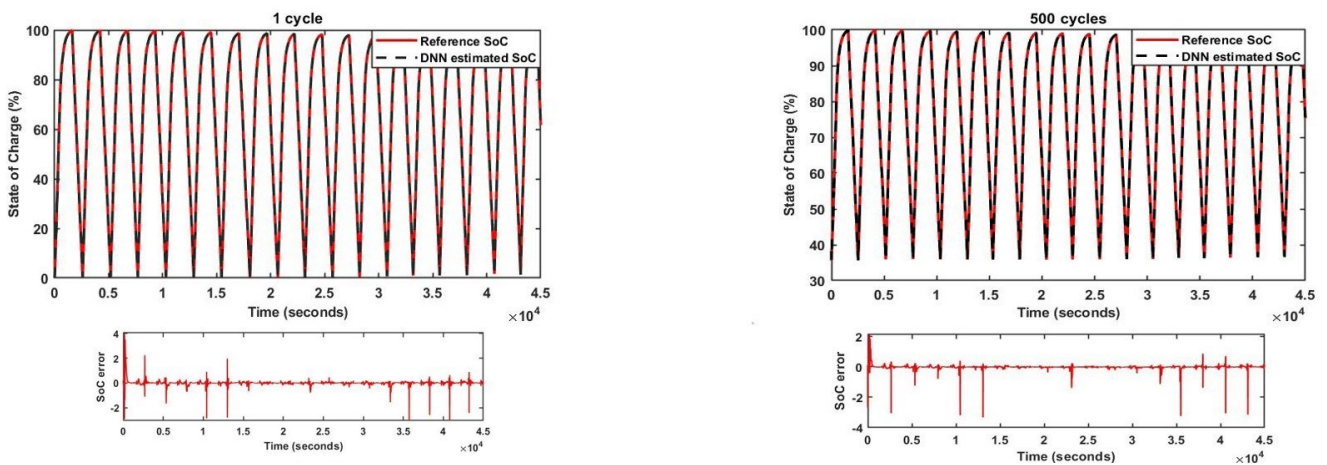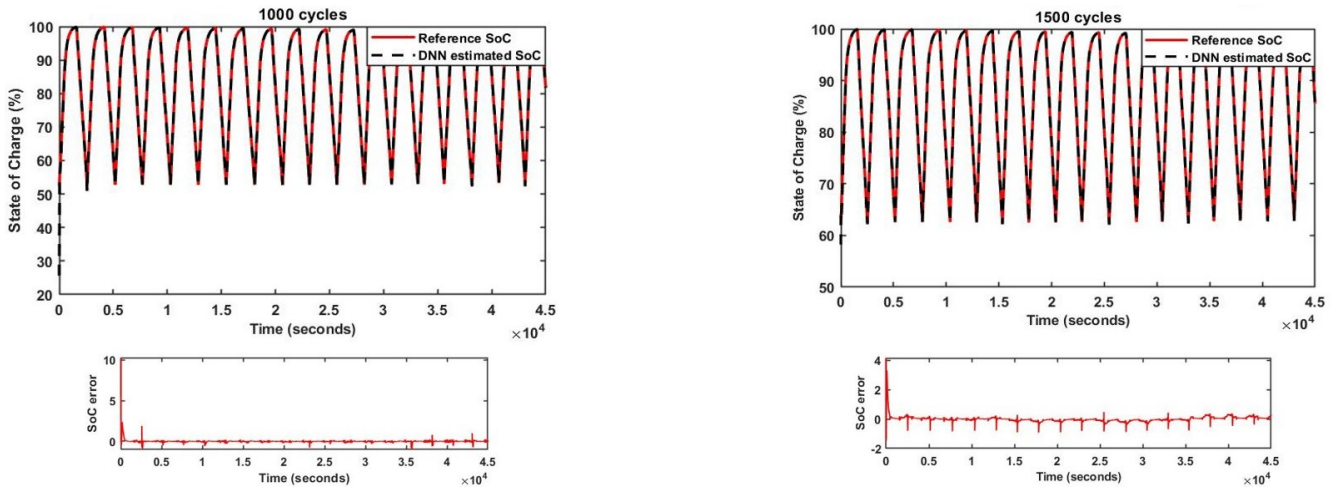

Figure 24. *Cont*.

Figure 24. Estimation of the SoC obtained at variable current using the DNN model with the aging effect.
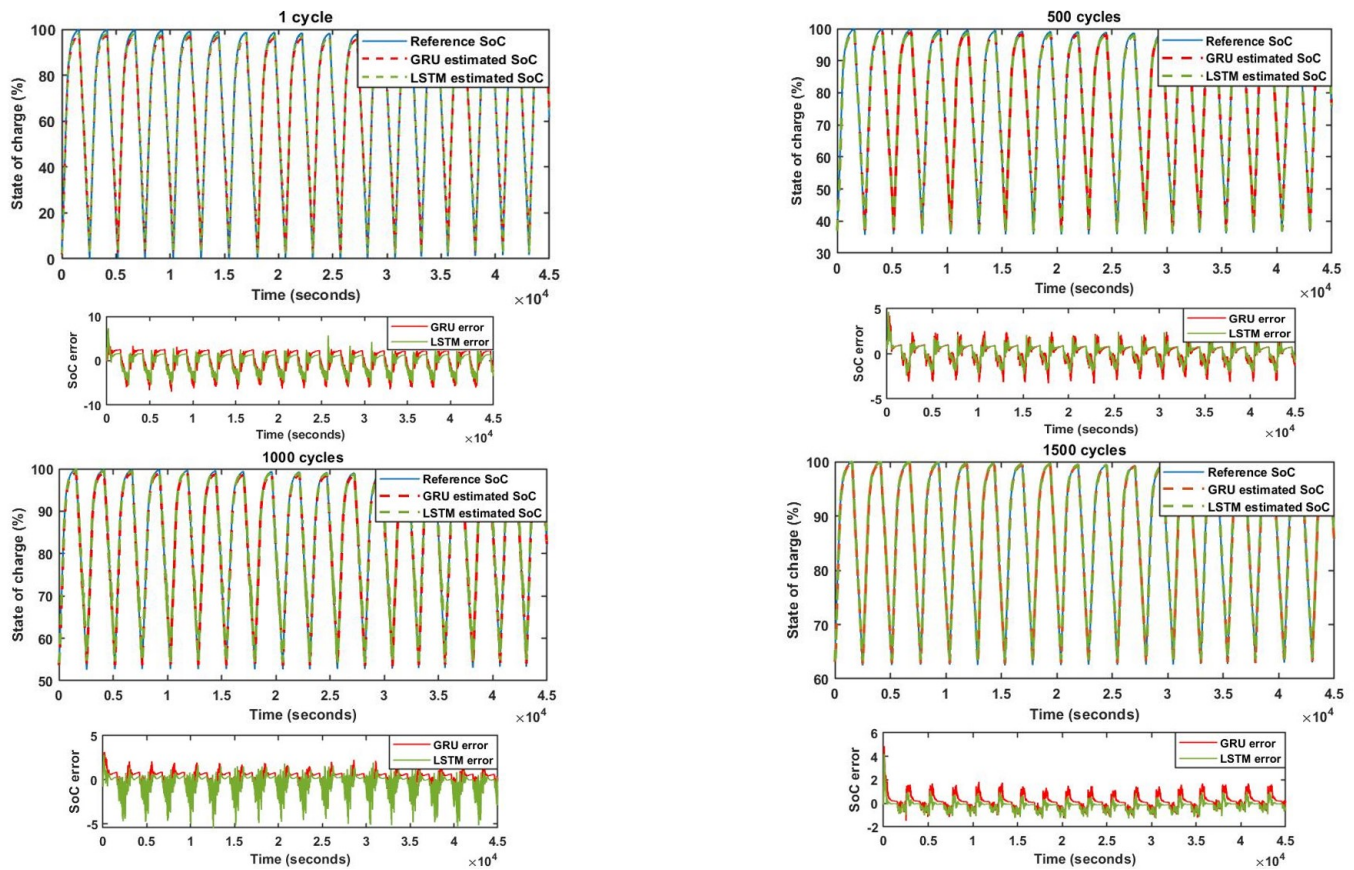

Figure 25. Estimation of the SoC obtained at variable current using the GRU and LSTM models with the aging effect.

The DNN model excels due to its ability to capture complex nonlinear relationships between input variables (current, voltage, temperature, aging effect) and output (SoC). The depth of the DNN enables it to extract relevant features at multiple levels of abstraction, improving the accuracy of SoC predictions. The DNN was trained with a diverse dataset covering different aging and temperature conditions, enabling the model to generalize efficiently. To avoid overlearning and improve model robustness, regularization techniques such as dropout were also used. The GRU is designed to model temporal sequences by capturing long-term dependencies in the data. The GRU is particularly effective for estimat-

ing the SoC because it can retain relevant information on previous charge and discharge cycles, which is crucial for predicting the actual state of the battery. The LSTM model is particularly suited for sequential prediction tasks due to its ability to store information over long periods and forget irrelevant information. This allows the LSTM model to effectively capture dynamic effects and complex interactions in battery cycles. The models were tested under different aging and temperature conditions to simulate real-life battery use scenarios. The results indicated that the DNN and LSTM model were particularly robust in the face of these variations, thanks to their ability to model complex relationships and store relevant information over long periods. The DNN achieved the best accuracy, with a maximum error of less than 2.5%. This can be attributed to the capacity of the DNN to capture complex features and its flexibility in terms of network structure. The GRU, although slightly less accurate than the DNN, offered a good compromise between performance and computation time, thanks to its simplified structure and its ability to capture temporal dependencies. The LSTM model, while offering robust performance due to its ability to handle long-term dependencies, was slightly slower to train than the GRU due to its increased complexity.

5. Conclusions

The accurate estimation of the SoC using deep learning algorithms is essential for a BMS to protect electric vehicle batteries against deep discharge and overcharging. In this paper, experimental data obtained using a reliable database were collected on a Panasonic UR18650ZY Li-ion battery, and simulation data using Matlab/Simulink software were used to test different profiles to ensure the reliability of the proposed models. A deep neural network (DNN), long short-term memory (LSTM) model, and gated recurrent unit (GRU) were used to estimate the SoC using both types of data to train, test, and validate each of the above models. A good correspondence in results was observed when comparing the estimated SoC with the real SoC, demonstrating the effectiveness of the suggested networks for learning the problem of estimating the SoC. Neural networks have proven their reliability, but the present DNN algorithm offered a robust and precise prediction for the battery sets used, with a mean error value under 0.5% and a maximum error value under 2.5%. Incorporating the effects of temperature and aging proved crucial to improving estimation accuracy, highlighting the importance of these factors often overlooked in previous studies. The future prospects of this research are promising. The results obtained can contribute to improving battery management systems in electric vehicles, thus increasing their efficiency and lifespan. In addition, this study paves the way for future research aimed at developing even more sophisticated neural network models, capable of handling varied and extreme conditions. Finally, although this study focused on lithium-ion batteries, the techniques developed can be adapted to other battery types, thus broadening the scope of this research.

The dynamics of batteries will be influenced by aging after a period of frequent use. In terms of perspectives, future research could consider the effect of battery aging to estimate the remaining useful life (RUL) and state of health (SoH) of different commercial battery cells. The software Matlab/Simulink will enable us to consider the effect of battery aging to improve the performance of SoH estimation methods. This work will concentrate on battery SoH estimation for electric vehicles based on deep learning algorithms (DNN), with the aim of developing a smarter combined method that incorporates the different models to create an even more accurate and efficient estimation model. This study will be followed by the realization and design of a BMS prototype in which the proposed methods will be executed and tested on a real electric vehicle and presented in a future research paper. However, it is important to note that high temperatures can also have negative effects on the performance and life of the battery. For example, it can lead to increased electrode and electrolyte wear, as well as increased corrosion and decomposition of battery materials. Therefore, it is important to consider the effects of high temperatures on overall battery performance and take steps in the future to minimize these negative effects, such as cooling the battery and reducing battery use at high temperatures.

Abbreviations

EV	Electric vehicle
RNN	Recurrent neural network
LSTM	Long short-term memory
MLP	Multilayer perceptron
GRU	Gated recurrent unit
RBF	Radial basis function
SoC	State of charge
UKF	Unscented Kalman filter
CC-CV	Constant current–Constant voltage
FFNN	Feedforward neural network
EKF	Extended Kalman filter
AGSMO	Adaptive Gain Sliding Mode Observer
APF	Adaptive particle filtering
NARX	Nonlinear autoregressive architecture with exogenous inputs
RMSE	Root-mean-square error
RFR	Random Forest Regressor
TBCC	Temperature-Based Coulomb Counting
DOB	Disturbance observer
PF	Particle filter
MAE	Mean absolute error
RLS	Recursive least square
H_∞	H-infinity
AEKF	Adaptive extended Kalman filter
SMO	Sliding Mode Observer
DNN	Deep neural networks
DTR	Decision Tree Regressor
ACKF	Adaptive curvature Kalman filter

Nomenclature

$Q(t)$	Electric vehicle
Q_n	Nominal capacity
x_i	Input from neuron of hidden layer i and neuron of hidden layer j
w_{ij}	Weight from neuron of hidden layer i to neuron of hidden layer j
R^2	Coefficient of determination
C_n	Nominal battery capacitor
$i(t)$	Battery's current at time t
g	Activation function
b_j	Bias of the hidden layer neuron j
w_h	Weight matrix between a hidden layer and an input layer
b_y	Hidden bias
y_k	RNN cell output at step k
H_k	Current hidden state

H_{k-1}	Previous state
b_h	Bias of the recurrent neuron
x_k	GRU gate input at step k
z_k	Update gate
r_k	Reset gate
$\hat{H}_k$	Candidate state
C_k	Hidden cell memory
f_k	Forget gate
o_k	Output gate
I_k	Current value of input vector
V_k	Voltage value of input vector
T_k	Temperature value of input vector

References

1. Scrosati, B.; Garche, J. Lithium batteries: Status, prospects and future. *J. Power Sources* **2010**, *195*, 2419–2430. [CrossRef]
2. Mwasilu, F.; Justo, J.J.; Kim, E.K.; Do, T.D.; Jung, J.W. Electric vehicles and smart grid interaction: A review on vehicle to grid and renewable energy sources integration. *Renew. Sustain. Energy Rev.* **2014**, *34*, 501–516. [CrossRef]
3. Yong, J.Y.; Ramachandaramurthy, V.K.; Tan, K.M.; Mithulananthan, N. A review on the state-of-the-art technologies of electric vehicle, its impacts and prospects. *Renew. Sustain. Energy Rev.* **2015**, *49*, 365–385. [CrossRef]
4. Lu, L.; Han, X.; Li, J.; Hua, J.; Ouyang, M. A review on the key issues for lithium-ion battery management in electric vehicles. *J. Power Sources* **2013**, *226*, 272–288. [CrossRef]
5. Ma, X.; Qiu, D.; Tao, Q.; Zhu, D. State of charge estimation of a lithium ion battery based on adaptive Kalman filter method for an equivalent circuit model. *Appl. Sci.* **2019**, *9*, 2765. [CrossRef]
6. Chemali, E.; Preindl, M.; Malysz, P.; Emadi, A. Electrochemical and electrostatic energy storage and management systems for electric drive vehicles: State-of-the-art review and future trends. *IEEE J. Emerg. Sel. Top. Power Electron.* **2016**, *4*, 1117–1134. [CrossRef]
7. McCurlie, L.; Preindl, M.; Emadi, A. Fast model predictive control for redistributive lithium-ion battery balancing. *IEEE Trans. Ind. Electron.* **2016**, *64*, 1350–1357. [CrossRef]
8. El Fallah, S.; Kharbach, J.; Rezzouk, A.; Ouazzani Jamil, M. Robust State of Charge Estimation and Simulation of Lithium-Ion Batteries Using Deep Neural Network and Optimized Random Forest Regression Algorithm. In Proceedings of the International Conference on Artificial Intelligence Industrial Applications 2023, Shenyang, China, 21–24 August 2023; Springer Nature: Cham, Switzerland, 2023; pp. 34–45.
9. Hasan, A.J.; Yusuf, J.; Faruque, R.B. Performance comparison of machine learning methods with distinct features to estimate battery SOC. In Proceedings of the 2019 IEEE Green Energy and Smart Systems Conference (IGESSC), Long Beach, CA, USA, 4–5 November 2019; pp. 1–5.
10. Lehmam, O.; El Fallah, S.; Kharbach, J.; Rezzouk, A.; Ouazzani Jamil, M. State of Charge Estimation of Lithium-Ion Batteries Using Extended Kalman Filter and Multi-layer Perceptron Neural Network. In Proceedings of the International Conference on Artificial Intelligence Industrial Applications 2023, Shenyang, China, 21–24 August 2023; Springer Nature: Cham, Switzerland, 2023; pp. 59–72.
11. Xing, L.; Wu, X.; Ling, L.; Lu, L.; Qi, L. Lithium battery SOC estimation based on multi-innovation unscented and fractional order square root cubature Kalman filter. *Appl. Sci.* **2022**, *12*, 9524. [CrossRef]
12. Kashkooli, A.G.; Fathiannasab, H.; Mao, Z.; Chen, Z. Application of artificial intelligence to state-of-charge and state-of-health estimation of calendar-aged lithium-ion pouch cells. *J. Electrochem. Soc.* **2019**, *166*, A605. [CrossRef]
13. Hannan, M.A.; Lipu, M.H.; Hussain, A.; Mohamed, A. A review of lithium-ion battery state of charge estimation and management system in electric vehicle applications: Challenges and recommendations. *Renew. Sustain. Energy Rev.* **2017**, *78*, 834–854.
14. Wang, Z.; Feng, G.; Zhen, D.; Gu, F.; Ball, A. A review on online state of charge and state of health estimation for lithium-ion batteries in electric vehicles. *Energy Rep.* **2021**, *7*, 5141–5161. [CrossRef]
15. Chen, X.; Shen, W.; Dai, M.; Cao, Z.; Jin, J.; Kapoor, A. Robust adaptive sliding-mode observer using RBF neural network for lithium-ion battery state of charge estimation in electric vehicles. *IEEE Trans. Veh. Technol.* **2015**, *65*, 1936–1947. [CrossRef]
16. Wang, C.; Zhang, X.; Yun, X.; Fan, X. A novel hybrid machine learning coulomb counting technique for state of charge estimation of lithium-ion batteries. *J. Energy Storage* **2023**, *63*, 107081. [CrossRef]
17. He, H.; Zhang, X.; Xiong, R.; Xu, Y.; Guo, H. Online model-based estimation of state-of-charge and open-circuit voltage of lithium-ion batteries in electric vehicles. *Energy* **2012**, *39*, 310–318.
18. Leksono, E.; Haq, I.N.; Iqbal, M.; Soelami, F.N.; Merthayasa, I.G.N. State of charge (SoC) estimation on LiFePO 4 battery module using Coulomb counting methods with modified Peukert. In Proceedings of the 2013 Joint International Conference on Rural Information Communication Technology and Electric-Vehicle Technology (rICT ICeV-T), Bandung, Indonesia, 26–28 November 2013; pp. 1–4.
19. Zhang, M.; Fan, X. Review on the state of charge estimation methods for electric vehicle battery. *World Electr. Veh. J.* **2020**, *11*, 23. [CrossRef]

20. Tran, M.K.; DaCosta, A.; Mevawalla, A.; Panchal, S.; Fowler, M. Comparative study of equivalent circuit models performance in four common lithium-ion batteries: LFP, NMC, LMO, NCA. *Batteries* **2021**, *7*, 51 [CrossRef]

21. Shi, Y.; Ahmad, S.; Tong, Q.; Lim, T.M.; Wei, Z.; Ji, D.; Zhao, J. The optimization of state of charge and state of health estimation for lithium-ions battery using combined deep learning and Kalman filter methods. *Int. J. Energy Res.* **2021**, *45*, 11206–11230.

22. Meng, J.; Luo, G.; Gao, F. Lithium polymer battery state-of-charge estimation based on adaptive unscented Kalman filter and support vector machine. *IEEE Trans. Power Electron.* **2015**, *31*, 2226–2238. [CrossRef]

23. Rezaei, O.; Rahdan, A.; Sardari, S.; Dahmardeh, M.; Wang, Z. A fuzzy robust two-stage unscented Kalman filter method for uncertainty and state of charge estimation of lithium-ion batteries. *J. Energy Storage* **2023**, *68*, 107883. [CrossRef]

24. Guo, X.; Xu, X.; Geng, J.; Hua, X.; Gao, Y.; Liu, Z. SOC estimation with an adaptive unscented Kalman filter based on model parameter optimization. *Appl. Sci.* **2019**, *9*, 4177. [CrossRef]

25. Xiong, R.; He, H.; Sun, F.; Zhao, K. Evaluation on state of charge estimation of batteries with adaptive extended Kalman filter by experiment approach. *IEEE Trans. Veh. Technol.* **2012**, *62*, 108–117. [CrossRef]

26. Shen, J.; Xiong, J.; Shu, X.; Li, G.; Zhang, Y.; Chen, Z.; Liu, Y. State of charge estimation framework for lithium-ion batteries based on square root cubature Kalman filter under wide operation temperature range. *Int. J. Energy Res.* **2021**, *45*, 5586–5601. [CrossRef]

27. Sun, D.; Yu, X.; Zhang, C.; Wang, C.; Huang, R. State of charge estimation for lithium-ion battery based on an intelligent adaptive unscented Kalman filter. *Int. J. Energy Res.* **2020**, *44*, 11199–11218. [CrossRef]

28. Chen, X.; Shen, W.; Cao, Z.; Kapoor, A. Adaptive gain sliding mode observer for state of charge estimation based on combined battery equivalent circuit model. *Comput. Chem. Eng.* **2014**, *64*, 114–123. [CrossRef]

29. Ren, L.; Zhu, G.; Wang, J.V.; Luo, B.; Kang, J. Comparison of robustness of different state of charge estimation algorithms. *J. Power Sources* **2020**, *478*, 228767. [CrossRef]

30. Chen, P.; Lu, C.; Mao, Z.; Li, B.; Wang, C.; Tian, W.; Xu, Y. Evaluation of Various Offline and Online ECM Parameter Identification Methods of Lithium-Ion Batteries in Underwater Vehicles. *ACS Omega* **2022**, *7*, 30504–30518. [CrossRef]

31. Xu, W.; Wang, S.; Jiang, C.; Fernandez, C.; Yu, C.; Fan, Y.; Cao, W. A novel adaptive dual extended Kalman filtering algorithm for the Li-ion battery state of charge and state of health co-estimation. *Int. J. Energy Res.* **2021**, *45*, 14592–14602. [CrossRef]

32. Lian, G.; Ye, M.; Wang, Q.; Wei, M.; Xu, X. Considering the temperature influence state-of-charge estimation for lithium-ion batteries based on a back propagation neural network and improved unscented Kalman filtering. *Int. J. Energy Res.* **2022**, *46*, 18192–18211. [CrossRef]

33. Sun, W.; Qiu, Y.; Sun, L.; Hua, Q. Neural network-based learning and estimation of battery state-of-charge: A comparison study between direct and indirect methodology. *Int. J. Energy Res.* **2020**, *44*, 10307–10319. [CrossRef]

34. Chai, H.; Gao, Z.; Jiao, Z.; Yang, C. State of charge estimation for lithium-ion batteries based on an adaptive fractional-order cubature Kalman filter with initial value compensation. *J. Energy Storage* **2023**, *68*, 107544. [CrossRef]

35. Ge, D.; Zhang, Z.; Kong, X.; Wan, Z. Online SoC estimation of lithium-ion batteries using a new sigma points Kalman filter. *Appl. Sci.* **2021**, *11*, 11797. [CrossRef]

36. Li, L.; Hu, M.; Xu, Y.; Fu, C.; Jin, G.; Li, Z. State of charge estimation for lithium-ion power battery based on h-infinity filter algorithm. *Appl. Sci.* **2020**, *10*, 6371. [CrossRef]

37. Yun, X.; Zhang, X.; Wang, C.; Fan, X. Online parameters identification and state of charge estimation for lithium-ion batteries based on improved central difference particle filter. *J. Energy Storage* **2023**, *70*, 107987. [CrossRef]

38. Meng, J.; Ricco, M.; Luo, G.; Swierczynski, M.; Stroe, D.I.; Stroe, A.I.; Teodorescu, R. An overview and comparison of online implementable SOC estimation methods for lithium-ion battery. *IEEE Trans. Ind. Appl.* **2017**, *54*, 1583–1591. [CrossRef]

39. Duong, V.H.; Bastawrous, H.A.; Lim, K.; See, K.W.; Zhang, P.; Dou, S.X. Online state of charge and model parameters estimation of the LiFePO4 battery in electric vehicles using multiple adaptive forgetting factors recursive least-squares. *J. Power Sources* **2015**, *296*, 215–224. [CrossRef]

40. He, H.; Xiong, R.; Zhang, X.; Sun, F.; Fan, J. State-of-charge estimation of the lithium-ion battery using an adaptive extended Kalman filter based on an improved Thevenin model. *IEEE Trans. Veh. Technol.* **2011**, *60*, 1461–146.

41. Plett, G.L. Extended Kalman filtering for battery management systems of LiPB-based HEV battery packs: Part 3. State and parameter estimation. *J. Power Sources* **2004**, *134*, 277–292. [CrossRef]

42. Campestrini, C.; Heil, T.; Kosch, S.; Jossen, A. A comparative study and review of different Kalman filters by applying an enhanced validation method. *J. Energy Storage* **2016**, *8*, 142–159. [CrossRef]

43. El Fallah, S.; Kharbach, J.; Hammouch, Z.; Rezzouk, A.; Ouazzani Jamil, M. State of charge estimation of an electric vehicle's battery using Deep Neural Networks: Simulation and experimental results. *J. Energy Storage* **2023**, *62*, 106904. [CrossRef]

44. Awadallah, M.A.; Venkatesh, B. Accuracy improvement of SOC estimation in lithium-ion batteries. *J. Energy Storage* **2016**, *6*, 95–104. [CrossRef]

45. Kim, I.S. The novel state of charge estimation method for lithium battery using sliding mode observer. *J. Power Sources* **2006**, *163*, 584–590. [CrossRef]

46. Messier, P.; Nguyen, B.H.; LeBel, F.A.; Trovao, J.P.F. Disturbance observer-based state-of-charge estimation for Li-ion battery used in light electric vehicles. *J. Energy Storage* **2020**, *27*, 101144. [CrossRef]

47. Oyucu, S.; Doğan, F.; Aksöz, A.; Biçer, E. Comparative Analysis of Commonly Used Machine Learning Approaches for Li-Ion Battery Performance Prediction and Management in Electric Vehicles. *Appl. Sci.* **2024**, *14*, 2306. [CrossRef]

48. Liang, Z.; Wang, R.; Zhan, X.; Li, Y.; Xiao, Y. Lithium-ion battery state-of-health prediction for new-energy electric vehicles based on random forest improved model. *Appl. Sci.* **2023**, *13*, 11407 [CrossRef]

49. Kang, L.; Zhao, X.; Ma, J. A new neural network model for the state-of-charge estimation in the battery degradation process. *Appl. Energy* **2014**, *121*, 20–27. [CrossRef]

50. Chen, Z.; Qiu, S.; Masrur, M.A.; Murphey, Y.L. Battery state of charge estimation based on a combined model of Extended Kalman Filter and neural networks. In Proceedings of the 2011 International Joint Conference on Neural Networks, San Jose, CA, USA, 31 July–5 August 2011; pp. 2156–2163.

51. Chemali, E.; Kollmeyer, P.J.; Preindl, M.; Emadi, A. State-of-charge estimation of Li-ion batteries using deep neural networks: A machine learning approach. *J. Power Sources* **2018**, *400*, 242–255. [CrossRef]

52. Tran, M.K.; Panchal, S.; Chauhan, V.; Brahmbhatt, N.; Mevawalla, A.; Fraser, R.; Fowler, M. Python-based scikit-learn machine learning models for thermal and electrical performance prediction of high-capacity lithium-ion battery. *Int. J. Energy Res.* **2022**, *46*, 786–794. [CrossRef]

53. El Fallah, S.; Kharbach, J.; Sassi, H.B.; Rezzouk, A.; Ouazzani Jamil, M. SoC estimation of Lithium-ion battery: Simulation and Comparative study of machine learning-based modelling methods. In Proceedings of the 1st International conference on physical and engineering sciences (ICPES'22), Istanbul, Turkey, 29–30 May 2022; p. 54.

54. Ma, L.; Hu, C.; Cheng, F. State of charge and state of energy estimation for lithium-ion batteries based on a long short-term memory neural network. *J. Energy Storage* **2021**, *37*, 102440. [CrossRef]

55. Hu, J.N.; Hu, J.J.; Lin, H.B.; Li, X.P.; Jiang, C.L.; Qiu, X.H.; Li, W.S. State-of-charge estimation for battery management system using optimized support vector machine for regression. *J. Power Sources* **2014**, *269*, 682–693. [CrossRef]

56. Hu, C.; Jain, G.; Zhang, P.; Schmidt, C.; Gomadam, P.; Gorka, T. Data-driven method based on particle swarm optimization and k-nearest neighbor regression for estimating capacity of lithium-ion battery. *Appl. Energy* **2014**, *129*, 49–55. [CrossRef]

57. Chaoui, H.; Ibe-Ekeocha, C.C. State of charge and state of health estimation for lithium batteries using recurrent neural networks. *IEEE Trans. Veh. Technol.* **2017**, *66*, 8773–8783. [CrossRef]

58. Maleki, S.; Ray, B.; Hagh, M.T. Hybrid framework for predicting and forecasting State of Health of Lithium-ion batteries in Electric Vehicles. *Sustain. Energy Grids Netw.* **2022**, *30*, 100603. [CrossRef]

59. Yang, F.; Zhang, S.; Li, W.; Miao, Q. State-of-charge estimation of lithium-ion batteries using LSTM and UKF. *Energy* **2020**, *201*, 117664. [CrossRef]

60. Dargan, S.; Kumar, M.; Ayyagari, M.R.; Kumar, G. A survey of deep learning and its applications: A new paradigm to machine learning. *Arch. Comput. Methods Eng.* **2020**, *27*, 1071–1092. [CrossRef]

61. Hannan, M.A.; Lipu, M.S.; Hussain, A.; Ker, P.J.; Mahlia, T.I.; Mansor, M.; Dong, Z.Y. Toward enhanced state of charge estimation of lithium-ion batteries using optimized machine learning techniques. *Sci. Rep.* **2020**, *10*, 4687. [CrossRef] [PubMed]

62. Jerouschek, D.; Tan, Ö.; Kennel, R.; Taskiran, A. Data preparation and training methodology for modeling lithium-ion batteries using a long short-term memory neural network for mild-hybrid vehicle applications. *Appl. Sci.* **2020**, *10*, 7880. [CrossRef]

63. Chen, J.; Feng, X.; Jiang, L.; Zhu, Q. State of charge estimation of lithium-ion battery using denoising autoencoder and gated recurrent unit recurrent neural network. *Energy* **2021**, *227*, 120451. [CrossRef]

64. Chen, J.; Lu, C.; Chen, C.; Cheng, H.; Xuan, D. An improved gated recurrent unit neural network for state-of-charge estimation of lithium-ion battery. *Appl. Sci.* **2022**, *12*, 2305. [CrossRef]

65. Hochreiter, S.; Schmidhuber, J. Long short-term memory. *Neural Comput.* **1997**, *9*, 1735–1780. [CrossRef]

66. Park, J.; Lee, J.; Kim, S.; Lee, I. Real-time state of charge estimation for each cell of lithium battery pack using neural networks. *Appl. Sci.* **2020**, *10*, 8644. [CrossRef]

67. Kalman, B.L.; Kwasny, S.C. Why tanh: Choosing a sigmoidal function. In Proceedings of the IJCNN International Joint Conference on Neural Networks, Beijing, China, 7–11 June 1992; Proceedings 1992; IEEE: Piscataway, NJ, USA, 1992; p. 57

68. Chang, W.Y. The state of charge estimating methods for battery: A review. *Int. Sch. Res. Not.* **2013**, *2013*, 953792. [CrossRef]

69. Tian, J.; Xiong, R.; Shen, W.; Lu, J. State-of-charge estimation of LiFePO4 batteries in electric vehicles: A deep-learning enabled approach. *Appl. Energy* **2021**, *291*, 116812. [CrossRef]

70. Saha, B.; Goebel, K. Battery Data Set. In *NASA Ames Prognostics Data Repository*; NASA Ames Research Center: Moffett Field, CA, USA, 2007. Available online: https://ti.arc.nasa.gov/tech/dash/groups/pcoe/prognosticdata-repository/ (accessed on 9 January 2019).

71. Bole, B.; Kulkarni, C.; Daigle, M. *Randomized Battery Usage Data Set*; NASA Ames Progn Res Center: Moffett Field, CA, USA, 2009.

72. Dos Reis, G.; Strange, C.; Yadav, M.; Li, S. Lithium-ion battery data and where to find it. *Energy AI* **2021**, *5*, 100081. [CrossRef]

73. Zhao, Z.; Panchal, S.; Kollmeyer, P.; Emadi, A.; Gross, O.; Dronzkowski, D.; David, L. 3D FEA Thermal Modeling with Experimentally Measured Loss Gradient of Large Format Ultra-Fast Charging Battery Module Used for EVs. *SAE Tech. Pap.* **2022**. [CrossRef]

74. Bais, A.R.; Subhedhar, D.G.; Joshi, N.C.; Panchal, S. Numerical investigation on thermal management system for lithium ion battery using phase change material. *Mater. Today Proc.* **2022**, *66*, 1726–1733. [CrossRef]

75. Jaidi, J.; Chitta, S.D.; Akkaldevi, C.; Panchal, S.; Fowler, M.; Fraser, R. Performance Study on the Effect of Coolant Inlet Conditions for a 20 Ah LiFePO4 Prismatic Battery with Commercial Mini Channel Cold Plates. *Electrochem* **2022**, *3*, 259–275. [CrossRef]

76. Chrenko, D.; Fernandez Montejano, M.; Vaidya, S.; Tabusse, R. Aging study of in-use lithium-ion battery packs to predict end of life using black box model. *Appl. Sci.* **2022**, *12*, 6557. [CrossRef]

77. He, Z.; Jiang, Y.; Li, Y.; Zhu, J.; Zhou, H.; Meng, W.; Dai, L. Carbon layer-exfoliated, wettability-enhanced, SO3H-functionalized carbon paper: A superior positive electrode for vanadium redox flow battery. *Carbon* **2018**, *127*, 297–304. [CrossRef]

78. Jiang, Y.; Cheng, G.; Li, Y.; He, Z.; Zhu, J.; Meng, W.; Wang, L. Promoting vanadium redox flow battery performance by ultra-uniform ZrO2@ C from metal-organic framework. *Chem. Eng. J.* **2021**, *415*, 129014. [CrossRef]

79. Birkl, C.R.; Roberts, M.R.; McTurk, E.; Bruce, P.G.; Howey, D.A. Degradation diagnostics for lithium ion cells. *J. Power Sources* **2017**, *341*, 373–386. [CrossRef]

80. Schmidt, A.P.; Bitzer, M.; Imre, Á.W.; Guzzella, L. Experiment-driven electrochemical modeling and systematic parameterization for a lithium-ion battery cell. *J. Power Sources* **2010**, *195*, 5071–5080. [CrossRef]

81. Keil, P.; Jossen, A. Aging of lithium-ion batteries in electric vehicles: Impact of regenerative braking. *World Electr. Veh. J.* **2015**, *7*, 41–51. [CrossRef]

82. Connor, W.D.; Advani, S.G.; Prasad, A.K. Adaptive Thermal Control of Cell Groups to Extend Cycle Life of Lithium-Ion Battery Packs. *Appl. Sci.* **2023**, *13*, 4681. [CrossRef]

83. Waldmann, T.; Wilka, M.; Kasper, M.; Fleischhammer, M.; et Wohlfahrt-Mehrens, M. Temperature dependent ageing mechanisms in Lithium-ion batteries–A Post-Mortem study. *J. Power Sources* **2014**, *262*, 129–135. [CrossRef]

84. Wang, Q.; Jiang, B.; Li, B.; Yan, Y. A critical review of thermal management models and solutions of lithium-ion batteries for the development of pure electric vehicles. *Renew. Sustain. Energy Rev.* **2016**, *64*, 106–128. [CrossRef]

85. Capron, O.; Jaguemont, J.; Gopalakrishnan, R.; Van den Bossche, P.; Omar, N.; Van Mierlo, J. Impact of the temperature in the evaluation of battery performances during long-term cycling—Characterisation and modelling. *Appl. Sci.* **2018**, *8*, 1364. [CrossRef]

86. Xu, S.; Zhou, J.; Zhou, F.; Liu, Y. State-of-charge estimation for LiNi0. 6Co0. 2Mn0. 2O2/graphite batteries using the compound method with improved extended Kalman filter and long short-term memory network. *Int. J. Energy Res.* **2021**, *45*, 6115–6138. [CrossRef]

87. Zhang, C.; Zhu, Y.; Dong, G.; Wei, J. Data-driven lithium-ion battery states estimation using neural networks and particle filtering. *Int. J. Energy Res.* **2019**, *43*, 8230–8241. [CrossRef]

88. Kingma, D.P.; Ba, J. Adam: A method for stochastic optimization. *arXiv* **2014**, arXiv:1412.6980.

89. Fasahat, M.; Manthouri, M. State of charge estimation of lithium-ion batteries using hybrid autoencoder and Long Short Term Memory neural networks. *J. Power Sources* **2020**, *469*, 228375. [CrossRef]

90. Chen, Z.; Zhao, H.; Shu, X.; Zhang, Y.; Shen, J.; Liu, Y. Synthetic state of charge estimation for lithium-ion batteries based on long short-term memory network modeling and adaptive H-Infinity filter. *Energy* **2021**, *228*, 120630. [CrossRef]

91. Li, L.; Wang, C.; Yan, S.; Zhao, W. A combination state of charge estimation method for ternary polymer lithium battery considering temperature influence. *J. Power Sources* **2021**, *484*, 229204. [CrossRef]

92. Li, K.; Zhou, F.; Chen, X.; Yang, W.; Shen, J.; Song, Z. State-of-charge estimation combination algorithm for lithium-ion batteries with Frobenius-norm-based QR decomposition modified adaptive cubature Kalman filter and H-infinity filter based on electro-thermal model. *Energy* **2023**, *263*, 125763. [CrossRef]

93. Liu, Y.; Shu, X.; Yu, H.; Shen, J.; Zhang, Y.; Liu, Y.; Chen, Z. State of charge prediction framework for lithium-ion batteries incorporating long short-term memory network and transfer learning. *J. Energy Storage* **2021**, *37*, 102494. [CrossRef]

94. Tong, S.; Lacap, J.H.; Park, J.W. Battery state of charge estimation using a load-classifying neural network. *J. Energy Storage* **2016**, *7*, 236–243. [CrossRef]